

Recent Progress in Piezo-Phototronic Effect Enhanced Solar Cells

Laipan Zhu and Zhong Lin Wang*

For third generation semiconductors, for example, wurtzite ZnO and GaN, a piezopotential will be induced in these non-centrosymmetric structures through applying a stationary deformation. The synchronous occupancy of semiconductor engineering, piezoelectric property, and optical excitation processes in these materials brings about outstanding device performances, such as promoting carrier creation, transfer, separation, or suppressing carrier recombination. Enormous research interests have been sparked in this emerging field known as the piezo-phototronic effect. This manuscript reviews the fundamental research progress in enhanced photovoltaic efficiency by this effect, which not only provides a comprehensive coverage of the theoretical and experimental works illustrating the basic physics for understanding the enhanced solar cells when an external mechanical strain is applied, but also gives new insight into designing high-performance solar cells.

1. Introduction

To cut carbon emissions and protect the atmospheric environment, fossil fuels are urgent to be replaced by renewable energy technologies.^[1,2] Among them, the photovoltaic (PV) technology has caused widespread concern to become a green energy source.^[3–5] Conversion efficiency (η), the most important parameter to evaluate a solar cell performance, represents how much the incident solar power is converted into the maximum output power. Recently, the calculated world record-efficiencies regarding to different widely used PV technologies are counted (Figure 1a). Theoretical analysis (Shockley–Queisser

(S–Q) limit) indicates that an ultimate efficiency of 33.7% can be realized at an optical absorption band edge of 1.34 eV (Figure 1a).^[3,4] However, on account of the inefficient optical absorption and carrier accumulation, the measured short circuit current (J_{sc}) is much lower than the predicted value. The open circuit voltage (V_{oc}) is evidenced as well to be lower than the S–Q limiting value due to recombination mechanisms, such as Auger, interface/surface, band tail recombination, etc.^[5–7] Moreover, because of the existence of series and shunt resistances, the fill factor (FF) will also be suppressed.^[8] From the above, for a given bandgap, the practical efficiencies are usually significantly lower than that obtained from the S–Q limit. Light management and carrier management are two main approaches to promote

the performance of the solar cells (Figure 1b), for instance, seeking for highly efficient light absorption materials, optimizing device structures, and even utilizing new photovoltaic mechanisms.^[4,9–11]

Recently, an increasing interest in piezotronics and piezo-phototronics accompanied by novel physical science and unprecedented device applications has been sparked.^[12–17] A static force induced piezopotential in the wurtzite structured crystal has appeared due to the lack of central symmetry. The generation of piezopotential influences largely on the transport of electrons and holes at the interface/junction, which can find applications in flexible wearable devices, human interface technologies, sensors, etc.^[13] Coupling the light excitation, the piezo-phototronic effect can also have a huge positive impact on the optoelectronic devices, for example, optical sensors,^[18,19] light emitting diodes (LED),^[20,21] photoelectric switches,^[22] and even spintronic devices.^[23] Recently, numerous researchers have demonstrated a strengthened performance of solar cells with the help of piezo-phototronic effect.^[14,24,25]

This paper gives a brief review of recent advances in improved photovoltaic technologies via the piezo-phototronic effect. First, the basic theory and working principles of the effect to boost the performance of several typical solar cells are presented. Then, the latest researches of piezo-phototronic effect enhanced solar cells with different nanoscale dimensions are reviewed from both theoretical and experimental aspects, highlighting the advantages and scientific significances of each approach. At last, a brief summary and some objective perspectives are provided. This review not only wants to present deliberately an extensive summary to the theoretical

Dr. L. Zhu, Prof. Z. L. Wang
CAS Center for Excellence in Nanoscience
Beijing Key Laboratory of Micro-nano Energy and Sensor
Beijing Institute of Nanoenergy and Nanosystems
Chinese Academy of Sciences
Beijing 100083, P. R. China
E-mail: zhong.wang@mse.gatech.edu

Dr. L. Zhu, Prof. Z. L. Wang
School of Nanoscience and Technology
University of Chinese Academy of Sciences
Beijing 100049, P. R. China

Prof. Z. L. Wang
School of Material Science and Engineering
Georgia Institute of Technology
Atlanta, GA 30332, USA

 The ORCID identification number(s) for the author(s) of this article can be found under <https://doi.org/10.1002/adfm.201808214>.

DOI: 10.1002/adfm.201808214

and experimental works in order to illustrate the basic physics for understanding this effect enhanced PV performance, but also lays a solid foundation for designing and fabricating future advanced PV devices.

2. Theory of Piezo-Phototronics

2.1. Piezoelectricity, Piezopotential, and Piezo-Phototronics

One of the common characteristics of the third generation semiconductors is that most of them have wurtzite structure. The breaking of cubic symmetry leads to new effects in conjunction with conventional semiconductor physics. Here, the wurtzite-structured ZnO is chosen as a typical example. The hexagonal-structured wurtzite crystal usually possesses a large anisotropic property. The lack of center symmetry in the crystal gives rise to piezoelectricity. Simply, the centers of positive Zn^{2+} cations and negative O^{2-} anions are overlapped with each other. Therefore, no polarization can be detected in the crystal without applied strain. However, the two centers shift reversely with a strain applied at the top of a tetrahedron, leading to a polarization (Figure 2a). Figure 2b shows the perfectly aligned ZnO nanowires (NWs) grown through solution processes. A macroscopic potential is induced by a continuous overlay of the dipole polarization in the ZnO crystal, which is the so-called piezopotential.^[12,13,26] The inner piezopotential keeps existence with the presence of stress, because it is created by the ionic charges. The applied strain and the doping density (i.e., the doping-induced carriers can screen the piezoelectric charges) result in the magnitude of the piezopotential.

A piezopotential distribution can be simulated regardless of the doping in ZnO NW.^[27–29] As shown in Figure 2c, an overall potential drop of ≈ 0.4 V is created with positive potential at +c side (Figure 2c).^[27] The introduction of this



Laipan Zhu received his B.S. degree in Physics Department from Shandong University in 2010 and his Ph.D. in Institute of Semiconductors, Chinese Academic of Sciences in 2015. Now he is an associate professor in Prof. Zhong Lin Wang's group in Beijing Institute of Nanoenergy and Nanosystems, Chinese

Academic of Sciences. His main research interests have been focused on the field of piezotronics, piezo-phototronics, and spintronics.



Zhong Lin Wang is the Hightower Chair in Materials Science and Engineering and Regents' Professor at Georgia Tech, the Chief Scientist and Director of the Beijing Institute of Nanoenergy and Nanosystems, Chinese Academy of Sciences. His discovery and breakthroughs in developing nanogenerators and self-powered nanosystems establish the principle and technological road map for harvesting mechanical energy from environmental and biological systems for powering personal electronics and future sensor networks. He coined and pioneered the field of piezotronics and piezo-phototronics.

Academic of Sciences. His main research interests have been focused on the field of piezotronics, piezo-phototronics, and spintronics.

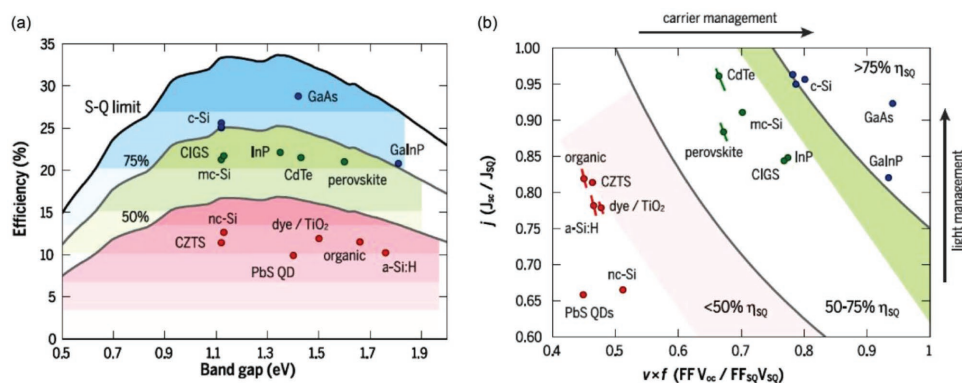


Figure 1. Comparison of different kinds of PV technologies. a) World record-efficiencies of different PV technologies compared to the theoretical S–Q efficiency limit as a function of bandgap. b) Comparison of the ratio (J_{sc}/J_{sq}) versus ($V_{oc} \times FF/V_{sq} \times FF$) for different kinds of record-efficiency cells. The two arrows indicate how much a specific PV material needs to improve regarding to light management and carrier management. Colors with red, green, and blue regions correspond to cells achieving $<50\%$, $50\text{--}75\%$, and $>75\%$ of their S–Q efficiency limit, respectively. Reproduced with permission.^[4] Copyright 2016, AAAS.

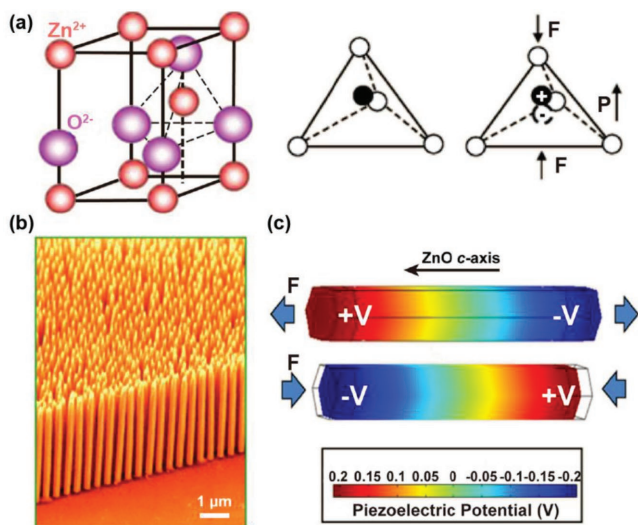


Figure 2. Piezopotential in wurtzite-structured ZnO nanowires. a) Schematic illustrations of the cellular distribution in ZnO, where F and P represent the applied stress and the induced electric dipole moment, respectively. b) Highly aligned ZnO nanowire arrays. Reproduced with permission.^[14] Copyright 2012, Wiley-VCH. c) Numerical piezopotential distributed in a c -axis ZnO NW under a stretched (upper one) or compressive (lower one) stress. Reproduced with permission.^[27] Copyright 2009, AIP.

piezoelectric potential along with the localized piezocharges distributed around the junction is the core for the emergence of piezo-phototronics, which optimizes effectively the optoelectronic properties of the PV materials. Hence, this effect couples three issues involving piezoelectric property, semiconductor engineering, and optical triggering process.^[13,14]

2.2. Material Systems for Piezo-Phototronics

1D nanomaterials are perfect candidates for their good mechanical endurance. ZnO, GaN, CdS nanowires/nanobelts are potential candidates for piezo-phototronics. So far, a popularly used material is ZnO NWs, which can be grown through a vapor-solid technology.^[14,30] The hydrothermal method is usually used to the preparation of ZnO NW arrays at less than 100 °C for several hours.

Recently, 2D MoS₂ with single-atomic-layer has also manifested a piezoelectric property,^[31] which reveals potential applications of 2D materials in powering nanodevices, wearable devices, and tactile sensors. Thanks to the excellent photoelectric, piezoelectric, and mechanical performances, it can be used for energy conversion and piezotronics,^[31–33] and even for high-performance piezo-phototronic solar cells.^[34]

Even in 3D bulk material grown with radio frequency (RF) magnetron sputtering, the piezoelectric property was also found, and the piezo-phototronic effect on a ZnO thin-film-based ultraviolet detector has been investigated.^[35] The enhancement in efficiency was also demonstrated in the ZnO thin film-based PV systems.^[36,37] Besides, thanks to the adjustable energy band, In_xGa_{1-x}N is an appealing material for PV technology,

and an improved efficiency of In_xGa_{1-x}N quantum well solar cell by an applied strain has indeed been observed.^[38–42]

2.3. Piezo-Phototronic Effect on Metal–Semiconductor Contact

Schottky barrier is derived from a contact between metal and semiconductor, which possesses rectifier properties.^[43,44] The height of Schottky barrier is usually not depended on the difference of work functions between the semiconductor and the metal.^[44–48] For a semiconductor with good piezoelectric property, thanks to the partial shielding of piezocharges, the remnant piezocharges can affect tremendously the nature of Schottky barrier. Due to the positive piezoelectric polarization under a tensile strain, the Schottky barrier height (SBH) is decreased, and the space charge zone is compressed (Figure 3a).^[13] On the contrary, an enhanced SBH and a widened depletion region are appeared with negative piezocharges at the interface (Figure 3b).^[13] Hence, the electronic transport is effectively manipulated by piezoelectric effect.^[13,14]

When photons whose energy surpasses the bandgap of the piezoelectric semiconductors irradiate on the metal–semiconductor contact, photoinduced carriers are created at the interface of the contact. The carriers are divided and gathered with the help of Schottky junction. Considering the case of n-type piezoelectric semiconductor, if its c -axis is oriented to the metal, positive piezocharges created under a tensile strain will lower the band profile, which weakens the dissociation of electron–hole pairs (Figure 3a). Hence, the entire accumulation of carriers is impeded. On the contrary, negative piezocharges caused under a compressive strain lift the band structure, which enhances the dissociation, movement, and accumulation of carriers (Figure 3b). While a dramatically lifted band when further increasing the strain will produce another potential barrier in valence band, which in turn inhibits the separation of electron–hole pairs.^[14,15]

2.4. Piezo-Phototronic Effect on p–n Junction

In a p–n junction with equilibrium state, an inner electric field and a charge depletion zone are created at the interface of the junction.^[43] Considering a n-type piezoelectric semiconductor, the space charge zone can be tuned by the incompletely screened piezocharges. For example, the band diagrams for a heterojunction structure are depicted, as shown in Figure 3c,d. The piezocharges distributed on the junction can manipulate the configuration of the space charge zone. Positive piezocharges under a tensile strain can lead to a narrowed and moved space charge zone (Figure 3c).^[49] The positive polarization charges lower the local energy band in the interface of the heterojunction, which constrains the dissociation or transfer of carriers. Conversely, negative piezocharges will make the space charge zone broadened and move to the n-type semiconductor (Figure 3d).^[49] A compressive stress results in a lifted band configuration (Figure 3d),^[14,50] leading to an enhanced carrier driving force. Hence, the dissociation or transportation of photoinduced carriers is strengthened.

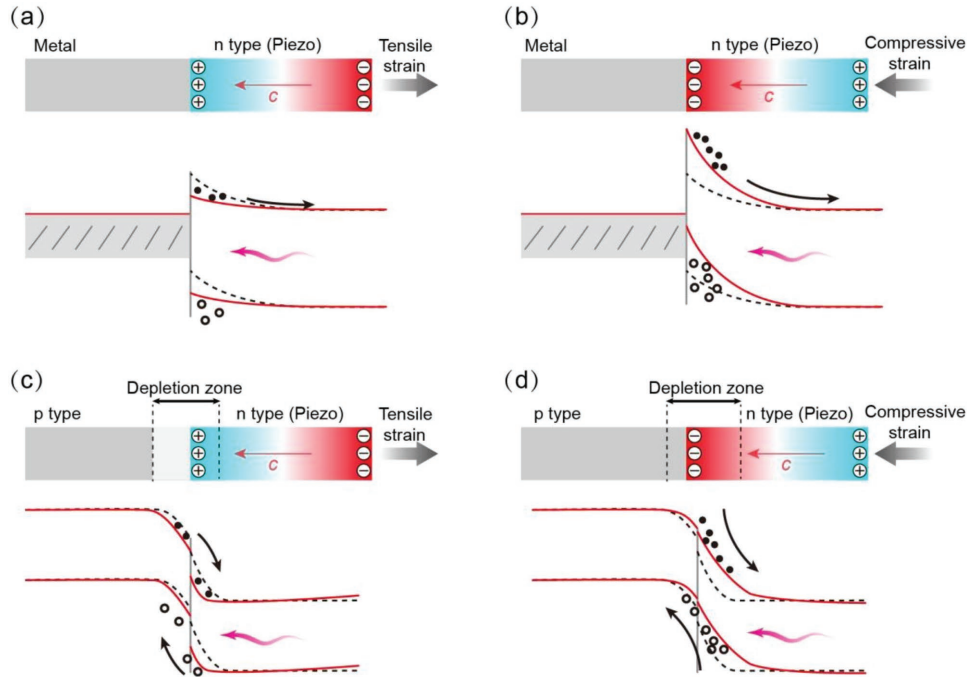


Figure 3. Schematic illustrations of energy band diagrams for the piezo-phototronic effect tuned M–S and p–n junction contacts. Enhanced performance of a) a M–S Schottky and c) a p–n junction device under a tensile strain. Reduced performance of b) a metal–semiconductor Schottky and d) a p–n junction device under a compressive strain. The color gradients illustrate the strain-induced piezopotential. Adapted with permission.^[15] Copyright 2016, Nature Publishing Group.

2.5. Basic Analysis Solutions for Piezo-Phototronic Effect on Solar Cells

Piezoelectric and semiconductor principles are applied to present the basic characteristics of a PV device consisting of a piezoelectric material.^[43,51–53] The theoretic frame of piezo-phototronics is established below by bringing the fundamental piezo-phototronic effect in PV devices. In a PV device, the huge built-in electric field in the space charge zone can help the dissociation of photoinduced carriers. The strain-induced piezocharges can prominently manipulate the band configuration, leading to a better optimization to the creation, dissociation, and transportation of photoinduced carriers, and therefore effectively regulate the PV characteristics.

The analysis results for ZnO piezoelectric p–n junction solar cells have been obtained.^[53] Given that the J_{sc} is stress free,^[53,54] the whole current density with piezoelectric polarization can be expressed as

$$J = J_{pn0} \cdot \exp\left[-\frac{q^2 \rho_{piezo} W_{piezo}^2}{2kT\epsilon_s}\right] \cdot \left[\exp\left(\frac{qV}{kT}\right) - 1\right] - J_{sc} \quad (1)$$

where ρ_{piezo} is the density of piezocharges, W_{piezo} is the width of the zone of the created piezocharges. Assuming that an abrupt junction distributes in the p-type semiconductor, the density of saturation current is written as

$$J_{pn} = J_{pn0} \cdot \exp\left[-\frac{q^2 \rho_{piezo} W_{piezo}^2}{2kT\epsilon_s}\right] \quad (2)$$

Here, $J_{pn0} = \frac{qD_n n_{p0}}{L_n} \cdot \exp\left[\frac{E_{F0} - E_i}{kT}\right]$ is the density of the saturation current, where E_{F0} , D_n , n_{p0} are the Fermi level without piezopotential, the electron diffusion coefficient, the electron concentration under the case of heat equilibrium, respectively.^[53]

Assuming $J = 0$, the V_{oc} can be deduced as $V_{oc} = \frac{KT}{q} \cdot \ln\left(\frac{J_{sc}}{J_{pn}} + 1\right)$. For the case of a typical solar cell, where $J_{sc} \gg J_{pn}$, it can then be approximately expressed as

$$V_{oc} \approx \frac{KT}{q} \cdot \ln\left(\frac{J_{sc}}{J_{pn}}\right) = \frac{KT}{q} \cdot \left[\ln\left(\frac{J_{sc}}{J_{pn0}}\right) + \frac{q^2 \rho_{piezo} W_{piezo}^2}{2kT\epsilon_s}\right] \quad (3)$$

The V_{oc} can be manipulated by the piezocharges created through the strain. The utilization of piezoelectric effect is not only suitable for 1D nano/microwire but also for 2D and even thin film materials.

Similar analysis is available for a Schottky solar cell. The saturation current density can be expressed as $J_{MS} = J_{MS0} \cdot \exp\left[\frac{q^2 \rho_{piezo} W_{piezo}^2}{2kT\epsilon_s}\right]$, where J_{MS0} denotes the case without piezoelectric charges and is written as

$$J_{MS0} = \frac{q^2 D_n N_c}{kT} \sqrt{\frac{2qN_D(\psi_{bi0} - V)}{\epsilon_s}} \left[\exp\left(\frac{-q\phi_{Bn0}}{kT}\right)\right] \quad (4)$$

where ψ_{bi0} and ϕ_{Bn0} are the built-in potential and SBH, respectively.^[53] Therefore, the open circuit voltage of the Schottky solar cell is expressed as

$$V_{oc} \approx \frac{KT}{q} \cdot \left[\ln \left(\frac{J_{sc}}{J_{MSO}} \right) - \frac{q^2 \rho_{piezo} W_{piezo}^2}{2kT\epsilon_s} \right] \quad (5)$$

These basic analyses depict the fundamental physics to comprehend the enhanced PV properties by the piezo-phototronic effect.^[55]

All the above discussions are assumed that the J_{sc} has no connection with the external strain.^[34,53,56,57] Weakening light reflection and enhancing light absorption are needed to promote J_{sc} .^[4] Luckily, nanostructure surfaces can validly reflect and limit light.^[58–60] Latest studies have evidenced that J_{sc} can also be enhanced by piezo-phototronic effect through applying an external strain on piezo-nanostructures.^[40,61–64] Improving the open circuit voltage needs detailed management to carrier recombination. Piezo-phototronic effect has been proven to have great potential to make the open circuit voltage improved. No matter if the J_{sc} is invariable with respect to the external strain, the V_{oc} can be modulated. It would be desirable that both J_{sc} and V_{oc} could be improved, but the answer which factor is dominant will depend on different material systems.

3. Theoretical Studies of Piezo-Phototronic Effect on Solar Cells with Different Nanoscale Dimensions

The following sections are some typical examples of theoretical studies of piezo-phototronic effect enhanced solar cells with different nanoscale dimensions. Although these solar cells are designed under relatively ideal conditions (ignoring many practical problems), it can guide us to understand new physics in

these novel structures and present new ideas for high performance solar cells in the future.

3.1. Theoretical Studies of Piezo-Phototronic Effect Enhanced Quantum Dot (QD) Solar Cells

Theoretically, the proposal of single-junction intermediate band solar cells (IBSCs) offers a supplementary method for PV devices.^[38,42,65,66] Due to the presence of discrete electron states, QD materials create intermediate band (IB), which provides three bands that are needed for an IBSC.^[41] Recently, Tang et al. studied theoretically the piezoelectric field dependence of InGaN QD-based IBSCs.^[41] As shown in Figure 4a, they designed an InGaN QDIBSC structure, which was supposed to be grown via a metal–organic chemical vapor deposition (MOCVD) technique. Their calculation based on $k \cdot p$ theory demonstrated that the optimal indium compositions for the barrier and the QDs were 0.4 and 0.8, respectively. And the height of QDs and the ratio of the QD bottom width to the top width were assumed to be 3 nm and 1:4, respectively, which was actually easy to be realized by MOCVD. As shown in Figure 4b, the piezoelectric fields can further push up the efficiency limit. A tenperiods of InGaN QD structure can enhance the conversion efficiency by 20% thanks to the existence of piezoelectric fields. Moreover, an optimal conversion efficiency of 46.0% was predicted with the absence of piezoelectric fields, while it elevated to 55.4% under a proper piezoelectric field. Figure 4c illustrated the distribution of the electric fields under a compressive strain, where the directions of piezoelectric fields in QDs were the same as that of the built-in electric fields derived from the p–n junction. Finally, an enhancement in builtin potential

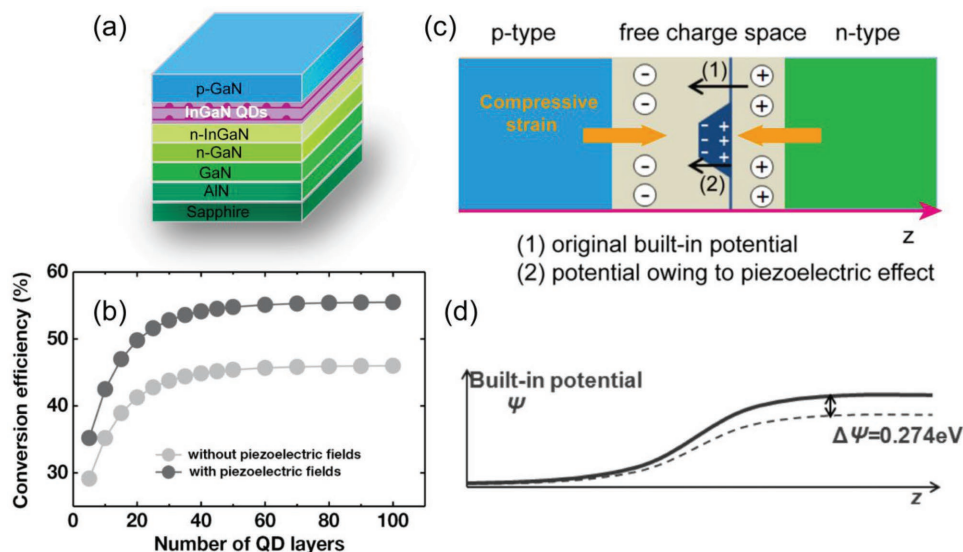


Figure 4. InGaN-based QD-IBSC under the influence of piezoelectric fields. a) Structure diagram of the device. b) Conversion efficiency as a function of number of QD layers with and without piezoelectric fields. c) The potential in the p–n junction of the InGaN-based QD-IBSC under a compressive strain. d) The builtin potential in the QD-IBSC with the piezoelectric fields considered (the solid line) and not considered (the dashed line), respectively. Reproduced with permission.^[41] Copyright 2015, IOP.

due to the stacked piezoelectric field was illustrated in Figure 4d. This work gives great guidance to the optimization of InGaN QD PV devices with an ultrahigh efficiency.

3.2. Theoretical Studies of Piezo-Phototronic Effect Enhanced NW Solar Cells

Recent theoretical researches indicated that, compared with thin films, NWs can bear greater lattice mismatch without creating defects.^[67–69] Theoretical analysis for comprehending the behavior of the extensively used piezoelectric NW solar cells is needed. In this section, we review two of the most successful theoretical studies of the enhanced NW solar cells via a strain.

3.2.1. InAs/InP Core/Shell NW Solar Cell

Self-assembled NWs can be used in solar cells with high energy conversion efficiency.^[70,71] Core-shell structured NWs were investigated previously as a good method in fabricating coaxial homojunctions,^[72] promoting the optical property of NWs,^[73] and optimizing energy gap via strain.^[74] Lattice mismatch in the core-shell NW results in a built-in electric field.^[55] This piezoelectric field is derived from the displacement of different atomic layers along the axis, which is present in both blended and wurtzite structures. In 2010, Boxberg et al. discovered in theory a piezoelectric performance in self-assembled InAs/InP NWs.^[55] The theoretical values of ϵ_{xx} and ϵ_{zz} in an^[110] oriented

InAs/InP NW were exhibited in Figure 5a,b, which were alike apart from a phase displacement of $\pi/2$. The strain was released effectively by surface expanding at the end of the NW. But the expanding effect influenced only on a small distance.

Figure 5c displayed the calculated surface piezoelectric charge density at a terminal surface of the NW. The density was negative on one terminal surface while positive on the other terminal surface, which diverged at the interface of the heterojunction with discontinuous relative dielectric constant. A piezopotential distributed at the cross profile of the InAs/InP NW was calculated (Figure 5d). Figure 5e illustrated an emerging photovoltaic property due to the piezoelectric field. Figure 5f showed a schematic diagram of applying piezoelectric core-shell NW arrays to large-area solar cells, where the photoinduced carriers were divided via the piezoelectric fields created under a strain.

3.2.2. Graded InGaN Nanowire Solar Cells

A reversed surface polarity in p-InGaN was predicted for In-rich cases, while the PV performance for In-rich InGaN was usually high.^[75] GaN/InGaN NW has demonstrated experimentally large dislocations and fractures with In component more than 0.25.^[76] Graded NW structure might be used to decrease the inner strain, making it possible for higher In component.^[77] Recently, Sarwar et al. found that the piezocharges can affect an unintentionally doped (UID)-In_xGa_{1-x}N NW PV device.^[78] Strain distribution in space in the NW was reckoned. A reduced performance of the PV device was demonstrated

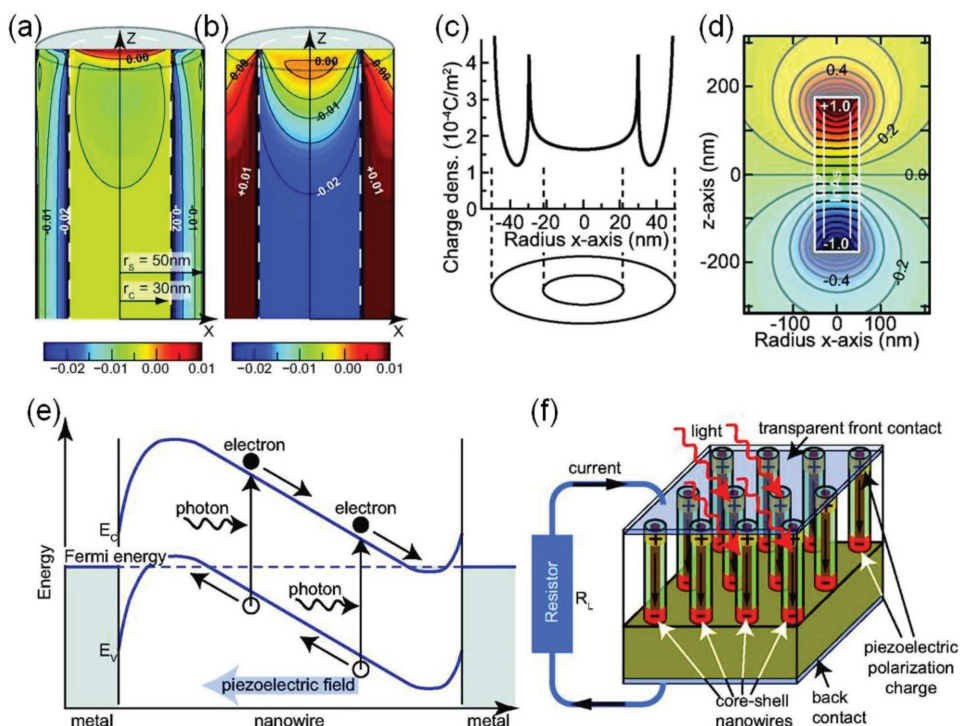


Figure 5. Piezo-phototronic effect on the^[110] oriented InAs/InP core/shell NW solar cell. a) Strain component ϵ_{xx} at an x - z cross-section. b) Strain component ϵ_{zz} at an x - z cross-section. c) Surface charge density and d) piezopotential distribution in the core-shell NW. e) Schematic energy band diagram of a NW photovoltaic device with piezoelectric field in NW as a driving force to separate the photoinduced carriers. f) Schematic PV device using piezoelectric field. Reproduced with permission.^[55] Copyright 2010, ACS.

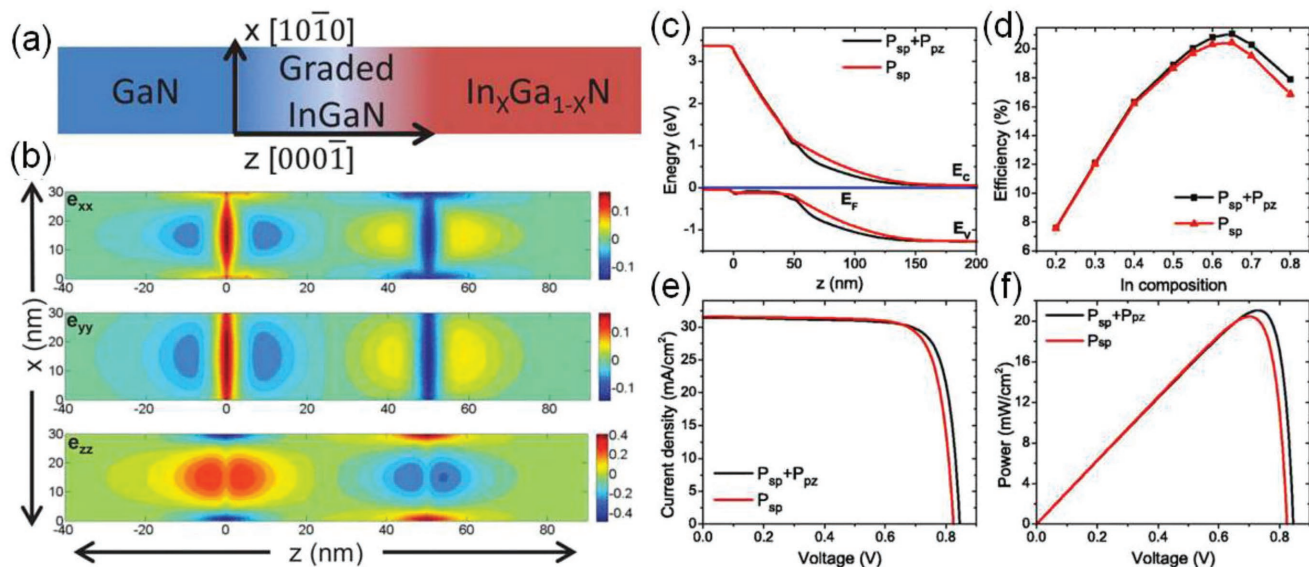


Figure 6. Piezoelectric effect on the graded InGaN NW solar cell. a) Schematic illustration of the structure of a graded InGaN NW. b) Distribution (in %) of strain components (e_{xx} , e_{yy} , and e_{zz}) of a GaN/ $\text{In}_{0.3}\text{Ga}_{0.7}\text{N}$ NW solar cell. c) Equilibrium energy band diagrams of p-GaN/UID-graded-InGaN/UID- $\text{In}_{0.65}\text{Ga}_{0.35}\text{N}$ NW solar cell. d) Efficiency for different In composition of the graded NW solar cell. e) J - V and f) P - V characteristics of the graded NW solar cell. P_{sp} corresponds to the case of only considering the spontaneous polarization charges, while $P_{sp} + P_{pz}$ corresponds to the case of considering both the spontaneous polarization and piezoelectric charges. Reproduced with permission.^[78] Copyright 2012, AIP.

due to piezoelectric polarization. However, an introduction of graded InGaN layer into the p-GaN/UID- $\text{In}_x\text{Ga}_{1-x}\text{N}$ made the performance of the device enhancing from <1% to 21%.

A UID-InGaN layer with 50 nm in thickness was inserted into the NW solar cell structure, as shown in Figure 6a. Spontaneous piezocharges were spread mainly over the graded layer. The strain distribution was calculated for the NW solar cell (Figure 6b). The largest components of strain were 0.18%, 0.18%, and 0.48% for e_{xx} , e_{yy} , and e_{zz} , respectively. Note that the entire largest component of strain was about six times less than that without the graded layer for a particular In component. A fluent optical transition from p-GaN to UID graded InGaN in the band scheme was sketched (Figure 6c). The In component dependence of the efficiency was illustrated in Figure 6d. A 21% supreme efficiency was obtained with In component of 65%. Piezoelectric charges increased the open circuit voltage which further enhanced the efficiency (see Figure 6e). The graded InGaN became p-type because of the piezoelectric charges in the graded component (Figure 6c). Piezoelectric charges boosted the inner electric field within the graded layer (Figure 6c). Hence, the efficiency of the PV device was enhanced. Figure 6f illustrated the voltage dependence of the power density in the graded PV device.

3.3. Theoretical Studies of Piezo-Phototronic Effect Enhanced Solar Cells Based on 2D Transition-Metal Dichalcogenides (TMDs)

2D TMD materials are fine candidates for designing flexible energy conversion devices, thanks to their outstanding optoelectronic characteristics.^[33,79–81] We take the monolayer MoS_2 as an example. First, monolayer MoS_2 within 1 nm can absorb up to 5% incoming sunlight.^[82] Second, it can bear a 11%

in-plane mechanical strain.^[83] Furthermore, it can be designed to be stacked PV devices.^[83] MoS_2 has also been proven to be a good piezoelectric semiconductor.^[31,84,85] Hence, monolayer MoS_2 single junction flexible solar cell might be improved effectively via piezo-phototronic effect.

Recently, a solar cell based on monolayer MoS_2 was studied theoretically, with a Schottky contact on the left side (Figure 7a).^[34] The piezocharges and piezopotential were applied to elevate or reduce the height of the Schottky barrier, as shown in Figure 7a,b. The modulation degree for the output performance has been investigated, and the V_{oc} was increased by 5.8% under a 1% strain. This method offers an effective way to optimize PV performances based on flexible 2D materials.

3.4. Theoretical Studies of Piezo-Phototronic Effect Enhanced Thin-Film Solar Cells

Recent advances indicated the piezoelectric characteristics of $\text{CH}_3\text{NH}_3\text{PbI}_3$ perovskite thin films.^[86–89] Piezo-phototronic effect enhanced $\text{CH}_3\text{NH}_3\text{PbI}_3$ perovskite PV device was studied at room temperature in theory.^[57] The ionic dipoles of this material were oriented in c -axis, and the piezoelectric modulus in this direction had been demonstrated to be about 0.83 C m^{-2} in former study.^[90] The thin film was sandwiched between CuI and TiO_2 .^[57] When a compressive or tensile strain was applied on the device, the piezoelectric polarization charges were induced on the upper and bottom surfaces of the perovskite thin film. By designing the upper metal–semiconductor contact ($\text{Au}/\text{CuI}/\text{CH}_3\text{NH}_3\text{PbI}_3$) as Schottky barrier, the piezocharges can modulate the barrier height.^[57] A ratio indicating how much the piezophototronic effect can affect the performance of a PV device was written as^[57]

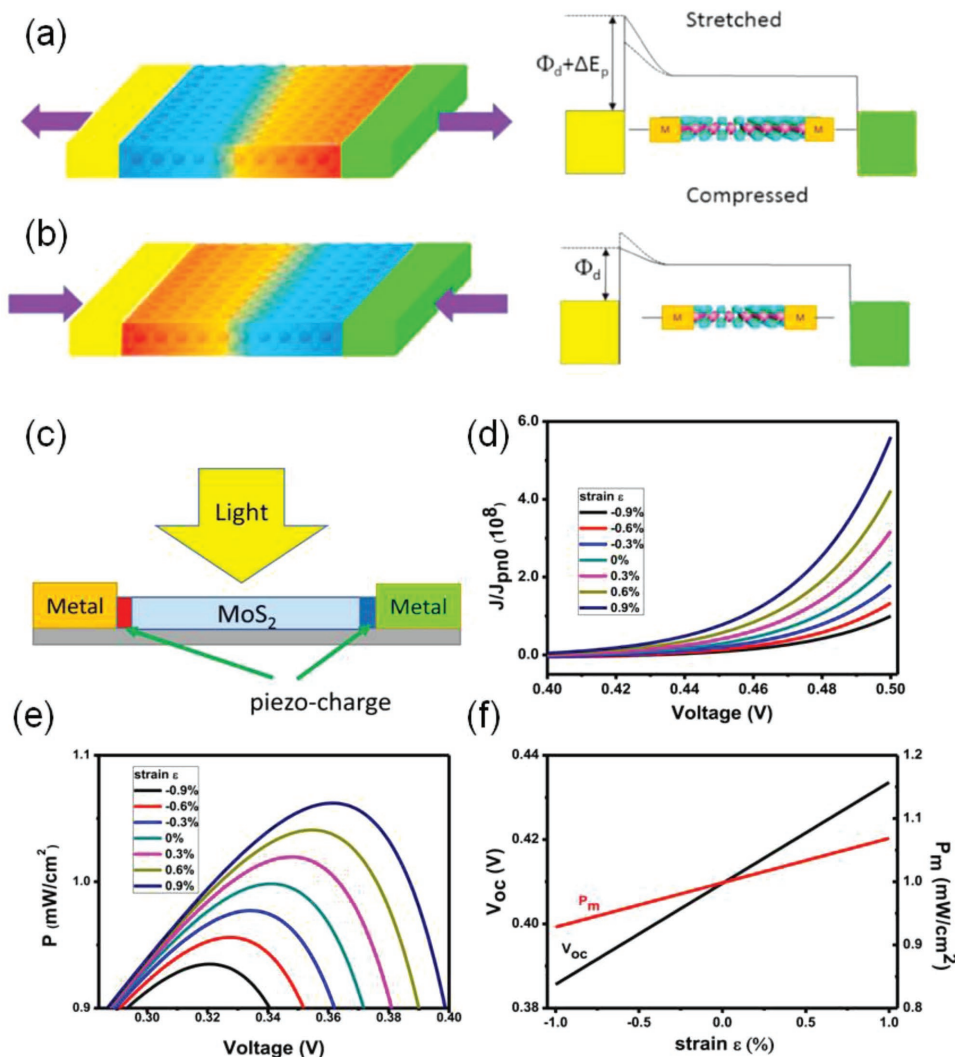


Figure 7. Monolayer MoS₂ Schottky solar cell under different strains. a) Schematic structure and energy band diagrams of a monolayer MoS₂ Schottky solar cell under a compressive strain. b) Schematic structure and energy band diagrams of the monolayer MoS₂ Schottky solar cell under a tensile strain. c) Schematic components of the monolayer MoS₂ Schottky solar cell. d) Relative current density and e) output power changing with the applied voltage under different strains. f) Open circuit voltage and maximum output power changing with the applied strains. Reproduced with permission.^[34] Copyright 2017, Elsevier Ltd.

$$\gamma = \frac{q^2 \rho_{\text{piezo}} W_{\text{piezo}}^2}{2kT\epsilon_s \ln\left(\frac{J_{\text{solar}}}{J_{\text{MS}}}\right)} \quad (6)$$

where J_{MS} is the saturation current density at the metal–semiconductor interface, J_{solar} is the short circuit current density, ρ_{piezo} is the density of the piezocharges, W_{piezo} is the width of charge distribution, k is the Boltzmann constant, T is the temperature, and ϵ_s is the dielectric constant. When W_{piezo} increases from 48 to 55 nm, the ratio γ was improved linearly from -1.56% to 1.79% . The theoretical analysis provides a future guidance for the design of perovskite solar cells with enhanced performance by using piezo-phototronic effect.

Moreover, Kazazis et al. have studied theoretically the PV properties in p–n and p–i–n GaN-based thin-film materials.^[38]

The beneficial manipulation of the piezocharges to the barrier height and carrier accumulation was elaborated. Considering a single p–n heterojunction, the efficiency was strengthened all the time with indium molar fractions (MFs) increasing to 0.5 under a consistent strain, which can be preserved (with MFs < 0.4) in the face of a partly released strain.^[38]

4. Experimental Studies of Piezo-Phototronic Effect on Solar Cells with Different Nanoscale Dimensions

Along with the theoretical studies, there is tremendous development in experimental studies. These experimental findings are in complete agreement with the above theoretical analysis and have recently been demonstrated in various

low-dimensional structures including quantum dots, nano-wires, nanowire arrays, and even thin films.

4.1. Piezo-Phototronic Effect Enhanced QD Solar Cells (QDSCs)

4.1.1. ZnO-Porous P(VDF-TrFE)/PbS QDSC

Colloidal quantum dots have potential applications in PV technology, due to its vast light absorption coefficient, tunable bandgap, and better compliance with solution method.^[91–94] However, many intrinsic defects are presented in these materials. The piezo-phototronic effect was proved to be a recommendable approach to solve this problem.^[14,50,95] Recently, Cho et al. inserted a layer of porous piezoelectric poly(vinylidene fluoride-trifluoroethylene) (P(VDF-TrFE)) polymer in the middle of n-ZnO and p-PbS, and the fabricated QDSCs were sketched in **Figure 8a**.^[95] The strain-induced piezopotential on P(VDF-TrFE) polymer modulated the performance of QDSCs. An increased J_{sc} by 37% was obtained under strain (Figure 8b). From Figure 8c,d, an applied compressive strain

created a piezopotential and modulated the depletion zone in contrast to a QDSC without applied strain. As a result, carrier's dissociation and collection were elevated at the interface. Oppositely, carrier's dissociation and collection were constrained under a tensile strain (Figure 8e). This study shows a potential application value of the piezo-phototronic effect in enhancing flexible colloidal QD PV devices.

4.1.2. ZnO /PbS QDSC

Depletion-heterojunction QDSCs are also a potential PV technology.^[96,97] In 2013, Wang and co-workers reported the investigation of optimized ZnO/PbS QDSCs by bringing piezocharges in the heterojunction interface.^[37] The efficiency of the QDSC was strengthened from 3.1% to 4.0% under a 0.25% compressive strain, and a linear dependence of the efficiency on strain was found. The strain-modulated $J-V$ characteristics were displayed in **Figure 9a**. The same variation tendency for the J_{sc} and efficiency was indicated with 0.51% and 0.55% change rate for each 0.01% strain, respectively (Figure 9b). Positive piezocharges

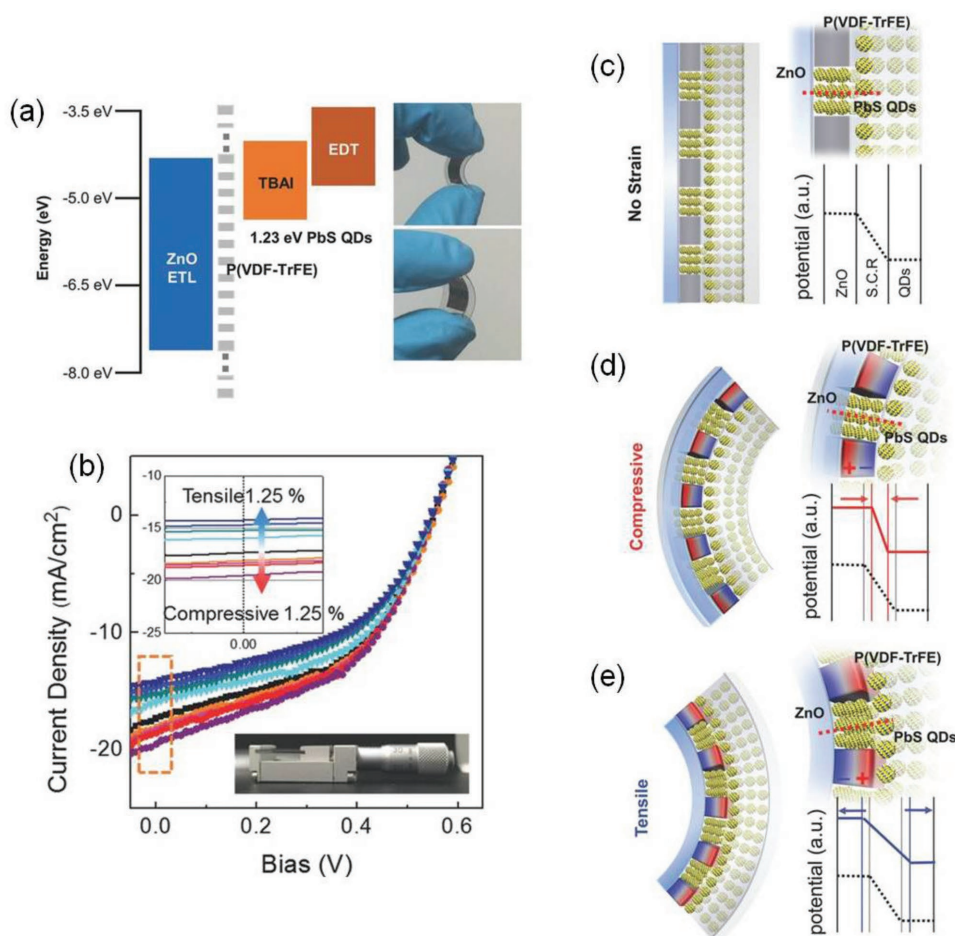


Figure 8. Strain dependence of a flexible PbS QDSC. a) Schematic energy band structure and real photographs of the PbS QDSC. b) $J-V$ characteristics of the solar cell under strains; the upper left and the bottom right insets show an enlarged J_{sc} for different strains and the configuration of device used for applying strain. c–e) Schematic diagrams indicating the modulated junctions by the piezopotential c) with no strain and under d) a compressive and e) a tensile strain, where S.C.R. denotes the space charge region. Reproduced with permission.^[95] Copyright 2018, WILEY-VCH.

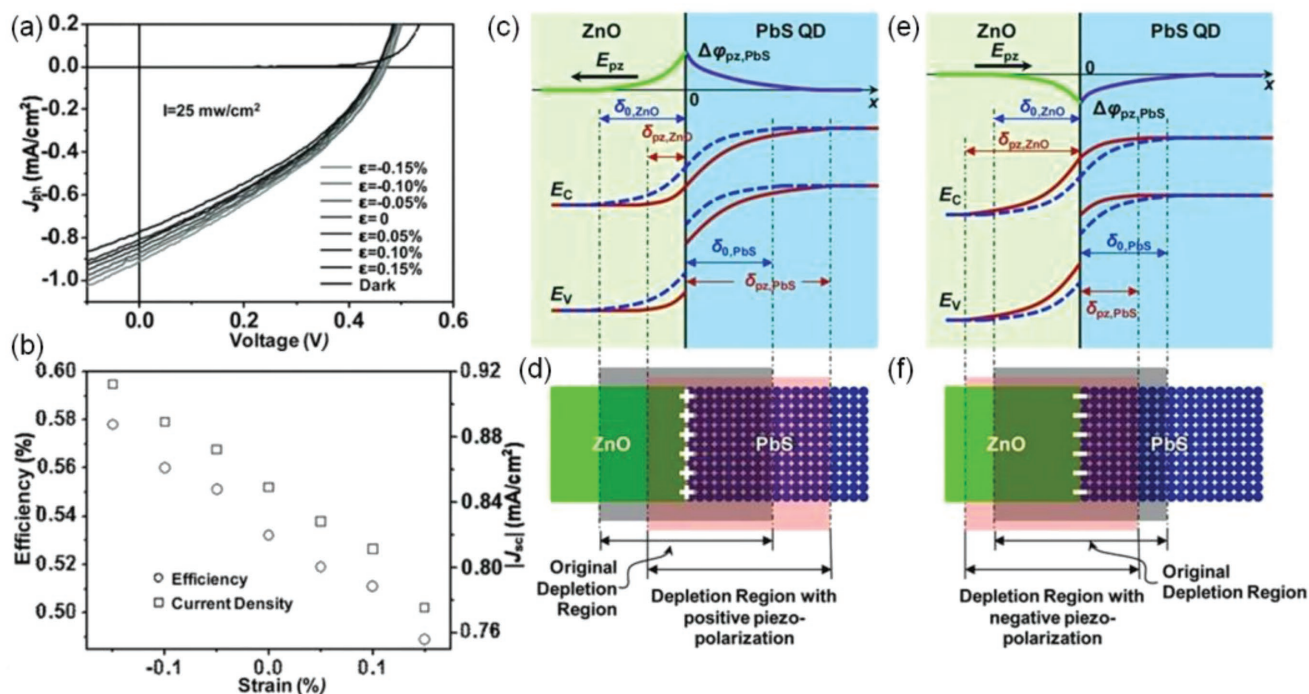


Figure 9. Piezo-phototronic effect on ZnO/PbS QDSC. a) J - V characteristics of a ZnO/PbS QDSC under different strains. b) Abstracted conversion efficiency and short circuit current changing with the applied strain. c,e) Schematic energy band diagrams of the QDSC with c) positive and e) negative piezocharges distributed at the ZnO/PbS interface, respectively. d,f) Schematic diagrams of the change of depletion regions with d) positive and f) negative piezocharges distributed at the ZnO/PbS interface, respectively. Reproduced with permission.^[37] Copyright 2013, WILEY-VCH.

induced near the interface lowered the bands, and the charge depletion region in the PbS QD layer was enlarged which was helpful for separation of carriers (Figure 9c,d). At the same time, a reduced space charge zone and lighter bending of band in ZnO were presented. A schematic variation of the entire modified space charge zone at the interface was exhibited in Figure 9d. Reversely, the band offset was reduced and the space charge zone in the PbS was shrunk when negative piezocharges appeared at the interface (Figure 9e,f). Hence, the carrier separation was suppressed and a reduced PV efficiency was measured.

4.2. Piezo-Phototronic Effect Enhanced Single Nanowire Solar Cells

Semiconductor nanowires possess great prospects for applications in PV devices, thanks to their better carrier collection, large relative surface area, and better light trapping properties. And the massive loss in efficiency due to surface/interface imperfection could be addressed using surface passivation technology and p-n junction engineering.^[98–102] Compared with Schottky/nanowire photocell,^[103] the heterojunction-based nanowire PVs can be fabricated with a more suitable range of light absorption. Interestingly, the piezo-phototronic effect introduced by applying an external deformation on piezoelectric semiconductor (like CdS, ZnO, and CdTe) can effectively promote the performance of PVs. In this section, we will review three kinds of solar cells based on single nanowire heterojunctions.

4.2.1. Cu₂S/CdS Coaxial Single Nanowire Solar Cells

The complex preparation methods and high production costs involved with chemical vapour deposition^[104] or metalorganic vapor-phase epitaxy^[105] limit the extensive application of coaxial NW. Luckily, the method of cation exchange reaction offers a simple and cheap way to fabricate high quality heteroepitaxy nanostructures.^[106,107] Pan et al. made a n-CdS/p-Cu₂S coaxial nanowire photovoltaic device using a cation exchange reaction.^[64,99] The wurzite-structured CdS has non-central symmetry, revealing good piezoelectric property.^[64,108] The fabrication processes were displayed in Figure 10a. A piezoelectric polarization was induced in CdS NW under an applied strain, which has an intense enhancement to the carrier transport properties.

The improved device performance under strains was investigated. Configuration I with Cu₂S distributed at the top section (Figure 10b) was studied. A lowered barrier height was demonstrated under a compressive strain (Figure 10c). And an I_{SC} and a V_{OC} of 0.25 nA and 0.26 V were created, respectively. The strain-modulated I - V characteristics of the device were indicated in Figure 10d. A large enhancement in the performance of this device was obtained, with a 32% enhancement of I_{SC} and a 10% increment of V_{OC} (Figure 10e). Therefore, the overall efficiency was promoted by 70% (Figure 10f). For the case of configuration II with Cu₂S distributed at the bottom section, however, the I_{SC} and the efficiency were weakened under a compressive strain.

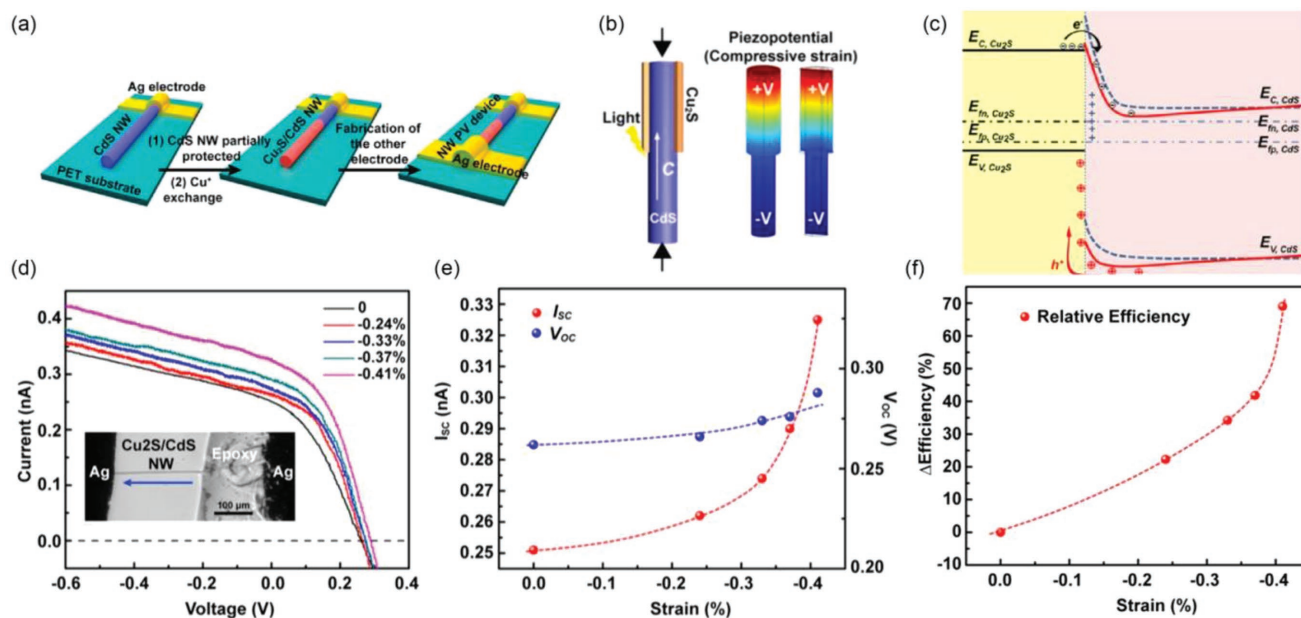


Figure 10. Performance of the CdS/Cu₂S coaxial NW solar cell modulated by the piezo-phototronic effect. a) Schematic fabrication processes of the PV device. b) Schematically calculated piezopotential distribution with a compressive strain. c) The strain-modulated energy band diagram. d) *I*–*V* curves of the solar cell under different compressive strain, where the inset denotes an optical micrograph of the solar cell. e) The *V*_{OC} and *I*_{SC}, and f) the relative efficiency tuned by the strain. Reproduced with permission.^[64] Copyright 2012, ACS.

4.2.2. P3HT/ZnO Single Nanowire Solar Cells

The polymer/inorganic semiconductor configuration is also a potential PV technology with versatile and flexible applicability.^[54,109–111] Yang et al. studied the strain-modulated solar cell manufactured with poly(3-hexylthiophene) (p-P3HT) and n-ZnO NW.^[54] A piezopotential distributed along [0001] orientation was calculated in a single ZnO micro/nanowire (Figure 11a,b). The tensile and compressive strains applied on the ZnO wire (with 1 and 10 μm in diameter and length, respectively) were 0.1% and –0.1%, respectively. The simulated piezopotential reached at 150 V, but in fact it should be much smaller by reason of the screening effect because of the free carriers.^[112] The positive piezocharges under a compressive strain lowered the band structure at the interface, leading to reduced ΔE and *V*_{OC} (shown in Figure 11a,c). Reversely, the negative piezocharges under tensile strains (Figure 11b) lifted the energy band at the interface, giving rise to elevated ΔE and *V*_{OC} (Figure 11d). As a result, the PV performance reduced/increased with elevated tensile/compressive strain (Figure 11e,f).

4.2.3. ZnO/Perovskite Single Nanowire Heterojunction Solar Cells

The outstanding properties such as long lifetime, large diffusion length, and high mobility make perovskite materials suitable for the utilization in solar cells, LED, photodetectors, lasers, etc.^[113–120] Recently, Hu et al. fabricated several ZnO/CH₃NH₃PbI₃ solar cells by selecting ZnO nanowire as an electron transport layer, and the modulation of performance by introducing externally strains to the devices was studied.^[63] For a ZnO NW with [0001]-direction oriented toward perovskite, the

*V*_{OC}, *I*_{SC}, and efficiency under a –0.8% strain were increased by 25%, 629%, and 1280%, respectively. This enhanced performance was derived from the effectively tuned energy band through piezoelectric charges and piezopotential near the interface of the ZnO/CH₃NH₃PbI₃ perovskite. It is the first experimental demonstration of perovskite PV devices improved by the piezo-phototronic effect.^[63] This experimental work provides a preferable approach for promoting the conversion efficiency of perovskite-based solar cells.

4.3. Piezo-Phototronic Effect Enhanced Planar Solar Cells Based on Nanowire Arrays

To enhance the density of photoinduced carriers, the introduction of antireflective and light-trapping layers is important.^[60,121,122] Fortunately, nanowire arrays possess these two properties,^[58,59,123] which is also simple and cheap to be fabricated compared with the vacuum-deposited technology. Moreover, as an effective approach, the piezo-phototronic effect has been extensively studied to improve the electrical transport properties based on piezoelectric NWs PV devices. Here, we will further review some kinds of planar solar cells based on nanowire arrays.

4.3.1. *p*⁺-Si/*p*-Si/*n*⁺-Si/*n*-ZnO NW Array Solar Cells

In recent decades, the silicon-based solar cells have become the mainstream in industrial community.^[4,124,125] Recently, we fabricated several monocrystalline silicon solar cells (Figure 12a) with areas of 1 cm × 1 cm by using ion-implanted technology, and we observed an increased efficiency thanks to

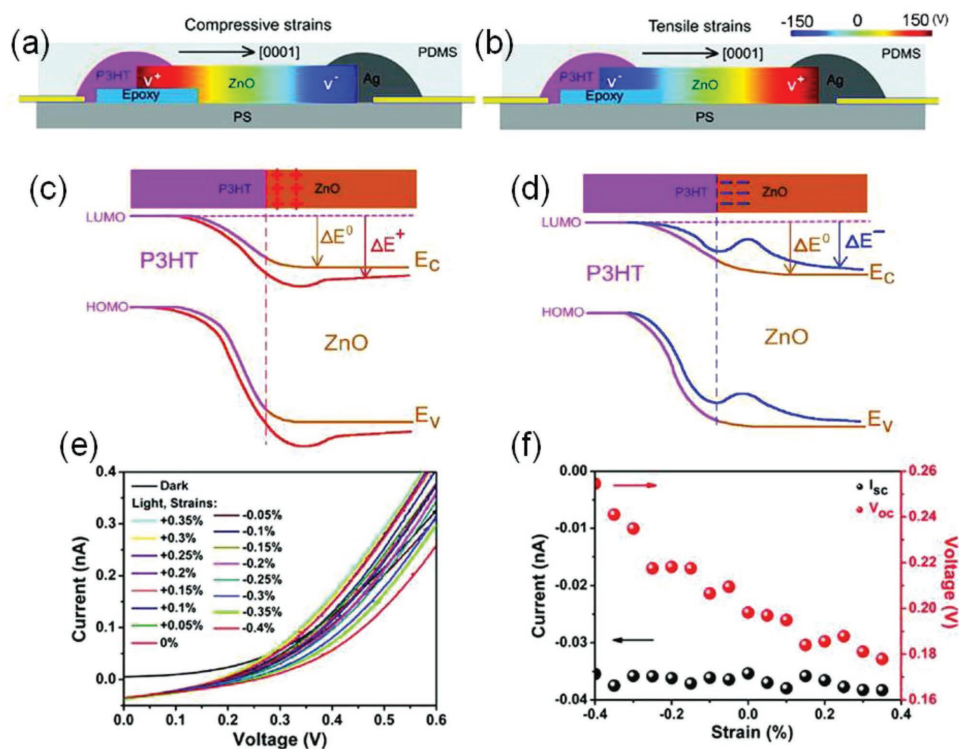


Figure 11. Piezo-phototronic effect on P3HT/ZnO NW solar cell. a,b) Calculated piezopotential distributions in the compressed and stretched device with [0001]-oriented ZnO NW. c) Schematic energy band diagram of the p-n junction with lowered band level and negative piezocharges at the space charge region. d) Schematic energy band diagram with raised band level and positive piezocharges at the space charge region. e) Strain modulated I - V characteristics of the solar cell. f) Strain modulated I_{sc} and V_{oc} of the solar cell. Reproduced with permission.^[54] Copyright 2011, ACS.

the introduction of ZnO NW arrays.^[62] The light absorption was enhanced intensely by the ZnO NW arrays. We measured the pressure-modulated J - V curves of the PV devices, as illustrated in Figure 12b,c. The detailed parameters as a function of vertical pressure were plotted in Figure 12d,e. A simultaneous increasing in the J_{sc} , V_{oc} , and FF with the increase of compressive pressure results in an improved efficiency from 8.97% to 9.51%. However, the efficiency started to reduce with further increasing the compressive pressure. On the other side, the efficiency under the tensile pressure of 300 KPa was degraded to 8.44%.

A good deal of photogenerated electrons were confined to the middle of n^+ -Si due to a disgusting surface barrier resulted from an ion implanted phosphorus ions. Figure 12f shows the schematic band structure. Under a compressive pressure, positive piezoelectric charges were created and distributed at the n^+ -Si/ZnO interface, lowering the surface barrier, therefore more electrons moved into n-ZnO (Figure 12g). The released electrons led to an increase in J_{sc} and V_{oc} . In addition, FF enhanced due to the weakened parasitic resistance. Therefore, the deduced efficiency was enhanced (Figure 12e). Because of the screening effect by free carriers, the variation of J_{sc} , V_{oc} , and FF was not pretty distinct under the applied strains.^[35,112,126] Whereas, the slant energy band began to constrain the electron transport by reasons of the increased piezopotential and the lowered potential well at the end of ZnO NW with an over 800 kPa pressure, therefore the efficiency dropped down when further increasing the pressure (Figure 12e). Conversely, negative piezocharges

distributed at the bottom part of the ZnO NWs were created under a tensile pressure, which raised the surface barrier at the interface of n^+ -Si/n-ZnO (Figure 12h). As a result, the trapping effect to photoinduced electrons was aggravated. Therefore, the energy conversion efficiency was decreased when increasing the tensile pressure (Figure 12e). Using optimal structures and shapes of piezoelectric nanostructures in the future, there still exists huge potential to further enhance the PV performance. This work shows industrial application prospects of the piezo-phototronic effect in large-scale silicon-based solar cells.

4.3.2. CIGS/CdS/n-ZnO NW Array Solar Cells

Cu(In,Ga)Se₂ (CIGS)-based thin film has now been developed into a promising material in flexible PV technology.^[59,127,128] Nevertheless, considering the high cost, there are urgent needs to find new ways to promote the efficiency. A CIGS/CdS/n-ZnO thin-film PV device enhanced by the piezo-phototronic effect thanks to ZnO thin film has been studied previously by Zhu et al., but the enhancement was comparatively small.^[129] In recent work, ZnO nanowire arrays with better piezoelectric property than ZnO thin films were applied to CIGS-based solar cells.^[61]

To explore in depth the physical mechanisms of the enhanced PV performance, energy band diagrams tuned by strain were illustrated (Figure 13a,b). When a compressive strain was exerted, positive piezocharges were created at the

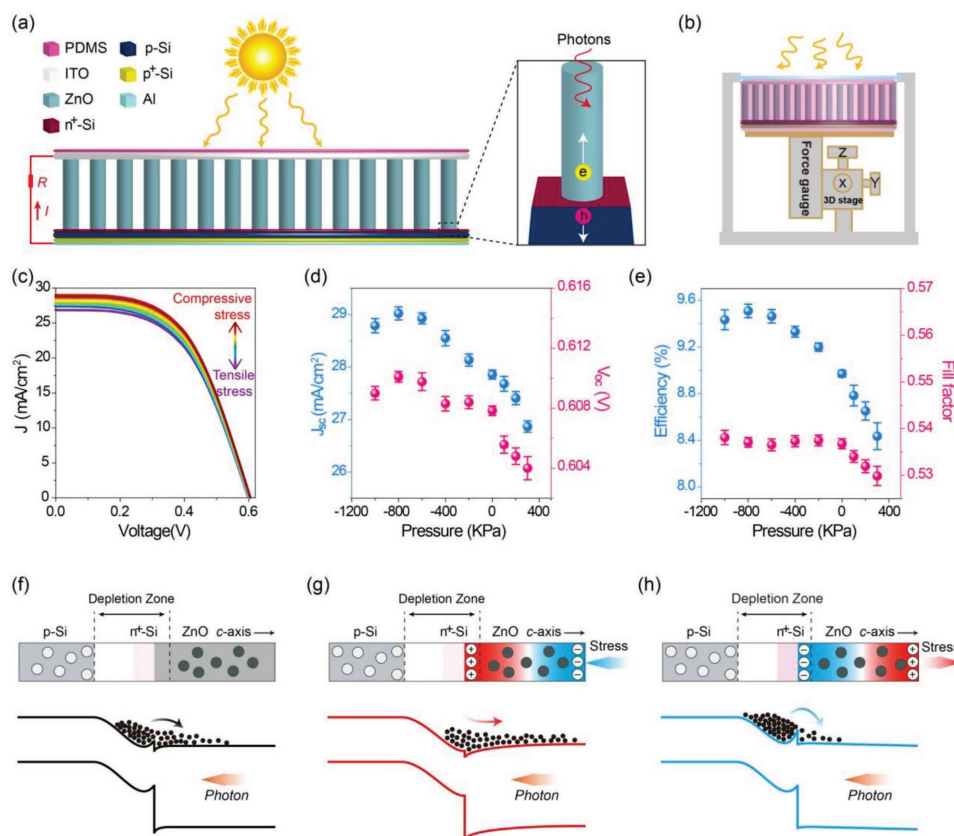


Figure 12. Piezo-phototronic effect on a silicon-based NW array solar cell. a) Schematic structural composition of the ZnO NW decorated silicon-based solar cell. b) Schematic illustration of the 3D force gauge used to supply vertical stress for the solar cell. c–e) Pressure modulated performances of the solar cell. f–h) Schematic diagrams of the tuned energy bands of the silicon-based NW array solar cell f) under no pressure, g) under a compressive pressure, and h) under a tensile pressure, respectively. Reproduced with permission.^[62] Copyright 2017, ACS.

“diffusion region II,” which led to a reduced band barrier at the ZnO/CdS interface, as shown in Figure 13a. Therefore, the dissociation of the carriers in the inner electric field was enhanced effectively. Oppositely, the interface bands of ZnO were raised up due to negative polarization charges when a tensile strain was applied, resulting in a lifted band barrier, as shown in Figure 13b. Finally, the J_{SC} and power conversion efficiency (PCE) were weakened.

The dependence of the PV parameters on the applied strain were presented in Figure 13c,d. With the strain varying from 0.8% to -0.8% , the V_{OC} and J_{SC} had an increment of 3.56% and 18.12%, respectively, however the FF always remained around 51%. Thanks to the combined improvement of both the V_{OC} and the J_{SC} , the PCE was enhanced effectively from 4.82% to 5.97% for an increment of 23.8%. This work demonstrates clearly that the piezo-phototronic effect via simply exerting force on ZnO nanowires can effectively be used for the CIGS-based flexible PV technology.^[61]

4.3.3. n-ZnO/p-SnS Core-Shell NW Array Solar Cells

Due to the large effective surface area, strong charge collection ability, and excellent light trapping properties,^[100,101,130] solar cells using core-shell NW arrays have become a big research

area for improving the PV performances.^[98,99] The core-shell morphology can promote the collecting efficiency of free charges by reasons of shortening the transport length of the free carriers, and optimizing the optical absorption.^[131] Zhu et al. fabricated a n-ZnO/p-SnS core-shell NW array solar cell, whose performance was proved to be elevated under a proper strain. SnS is an ideal shell material with a suitable optical bandgap for light absorption.^[132] Similar study on a ZnO/P3HT NW array solar cell improved by piezo-phototronic effect through an oscillating acoustic vibration was also explored.^[133]

Next, the device J - V characteristics modulated by bending strain were investigated (Figure 14a). An opposite polarization distribution was illustrated for the two different bending cases, as shown in Figure 14b. An enhanced performance was revealed when a compressive strain was applied while decreased for a tensile strain. Figure 14c,d showed the strain dependence of J_{SC} , V_{OC} , and FF. The J_{SC} reduced from 4.71 to 4.63 mA cm^{-2} , and the V_{OC} diminished from 0.58 to 0.51 V, while the FF remained around 0.48 when the strain were tuned from -0.88% to 0.88%. Therefore, a 8.3% enhancement in efficiency was observed with the compressive strain increasing from 0% to -0.88% (see Figure 14b).

There were lifted energy bands in space charge zone due to the compressive strain-induced negative piezocharges on the upper end of ZnO, as denoted in Figure 14e₁. This made the

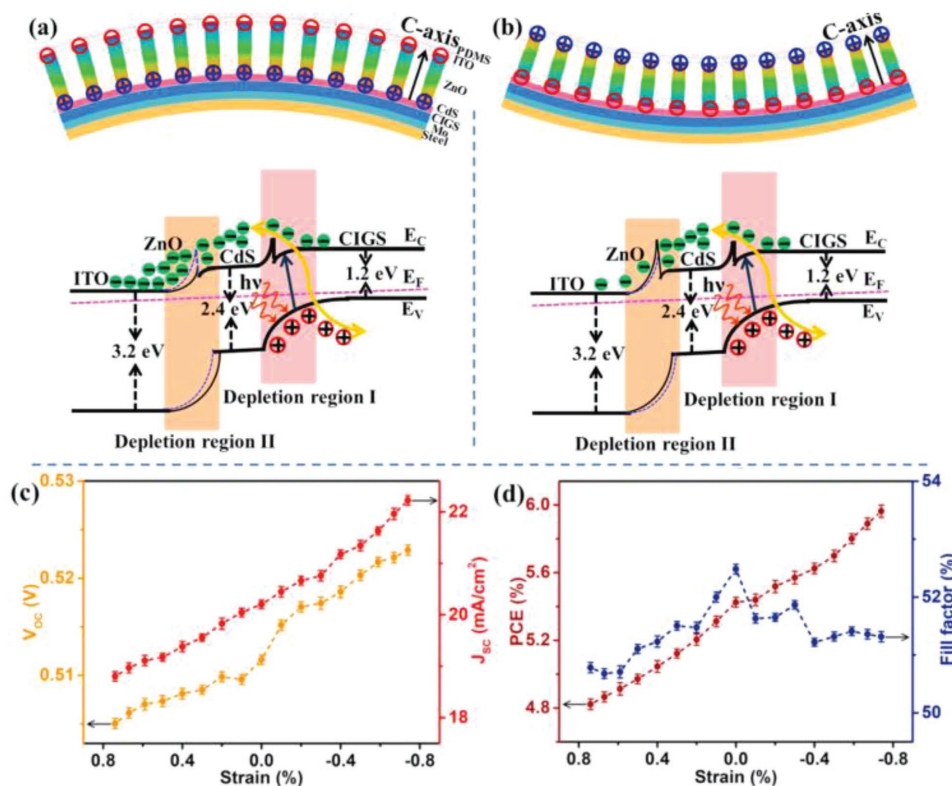


Figure 13. Piezo-phototronic effect on a flexible CIGS solar cell. a,b) Schematic structure and band diagrams under a) an upward bending and b) a downward bending. c,d) External strain dependence of c) the PCE and fill factor, and d) the V_{oc} and J_{sc} . Reproduced with permission.^[61] Copyright 2018, Elsevier Ltd.

photogenerated carriers separated easily by enlarging the width of the depletion zone and the strength of the internal field. And the piezopotential induced in ZnO NW was further worked to drive the transport of electrons. Moreover, although there was no piezoelectric charge at the side interface of ZnO/SnS core-shell nanowire, the transport of the carriers was also enhanced via the piezopotential presented in ZnO (Figure 14e₂). Based on these two mechanisms, the photoinduced current was lifted up with an applied compressive strain.

4.4. Piezo-Phototronic Effect Enhanced Thin-Film Solar Cells

In recent years, bulk thin films with wurtzite structure have also been proven to be good piezoelectric material systems.^[36,66,129] Wen et al. has explored the piezo-phototronic effect improved thin-film solar cells, where a nZnO film was grown using RF magnetron sputtering and then a light absorption layer p-P3HT was spin-coated on the nZnO film.^[36] An optimal enhanced performance on the PV device was obtained under a 0.32% tensile strain.^[36] In our previous work, we also found a weakly enhanced performance of a CIGS thin film solar cell by this effect, thanks to the ZnO piezoelectric thin film deposited by RF sputtering.^[129] Here, we will review concretely a recent work on piezo-phototronic effect enhanced PV device based on InGaN/GaN multiple quantum wells (MQWs).^[40]

Figure 15 revealed the device performance under different strains.^[40] The current density was enhanced with the increase of external applied strain (Figure 15a). From the P - V curves (Figure 15b), the voltage corresponding to the maximum power was almost the same, however the maximum power was enhanced when raising the external strain. The J_{SC} and the V_{OC} changing with the external strain were plotted (Figure 15c). The V_{OC} was almost invariant under different external strains due to the unchanged quasi-Fermi level splitting. While the J_{SC} was increased obviously due to the elevated light absorption. The maximum efficiency was promoted from 1.12% to 1.24% for a 11% increment under a 0.134% compressive strain. From Figure 15d, we can see that the FF reduced a little from 57.3% to 56.7%. The efficiency began to fall off once the applied strain reaching to 0.117% due to a stronger lattice scattering.

A symmetrically distributed pressure was applied on the c -axis (Figure 15e). The external piezocharges under pressure were created at the interfaces between the barriers and wells (Figure 15f). These external piezocharges partially offset the built-in charges generated due to lattice-mismatch.^[134] Furthermore, the carrier's wave functions moved into the well. Thus, increasing with the strain, the enhanced light absorption due to the stacking of wave functions resulted in much more photogenerated carriers. This work reveals great scientific significances in the research of basal physics and industrial applications of solar cells based on III-nitride thin-film semiconductors.

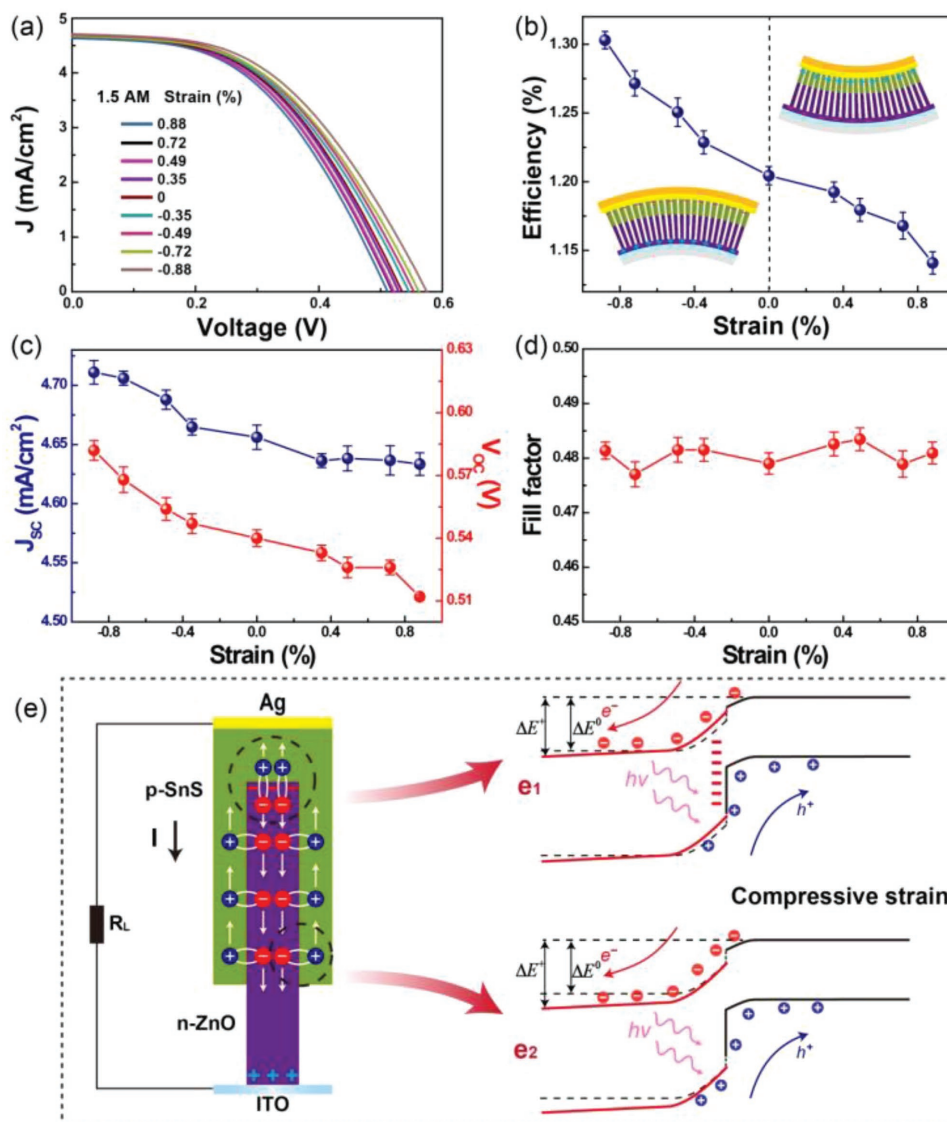


Figure 14. Piezo-phototronic effect on a ZnO/SnS core-shell NW array solar cell. a) J - V characteristics of the strain-modulated solar cell. b-d) Dependence of the PV parameters on bending strain. e) Schematic separation and transport (left side) of the photogenerated carriers in the core-shell NW and modulated energy band diagrams (e_1 and e_2) under a compressive strain. Reproduced with permission.^[132] Copyright 2017, WILEY-VCH.

5. Summary and Perspectives

In conclusion, the piezo-phototronic effect is a universal effect that applies to a range of materials that are lacking of centrosymmetry. This effect plays a unique role in the third generation semiconductors. Here, the applications of the piezo-phototronic effect in optimizing the performances of various solar cells are reviewed. First, we introduce the basic principles of this effect on PV devices in view of Schottky and p-n junctions. Then, we review recent progress in this effect enhanced PV technologies from both theory and experiment aspects and from the perspective of different nanoscale dimensions of piezoelectric semiconductors. The description of the effect offered in this review provides a new perspective on promoting the performances of solar cells by simply applying an external strain, which is very important for the development

of QD-, NW-, NW array-, and thin film-based solar cells. For low-efficiency solar cells with good flexibility, they have potential applications in curly buildings, flexible electronic devices, flexible power sources, and so on.

As for the solar cell materials that do not have the piezoelectric property, a thin layer of transparent ZnO nanostructures can be grown on the top surface, using which, the performance of the solar cell below can be tuned by the influence of the piezoelectric effect from the ZnO. Furthermore, ZnO nanostructures can be easily grown in large quantities with low-cost methods on any shape of substrate, showing great biologically compatible and environmentally friendly properties. This gives a future perspective that we can rationally introduce a thin layer of transparent piezoelectric ZnO nanostructures on the surface of solar cell materials, which not only remains the original performance of the PV devices but also

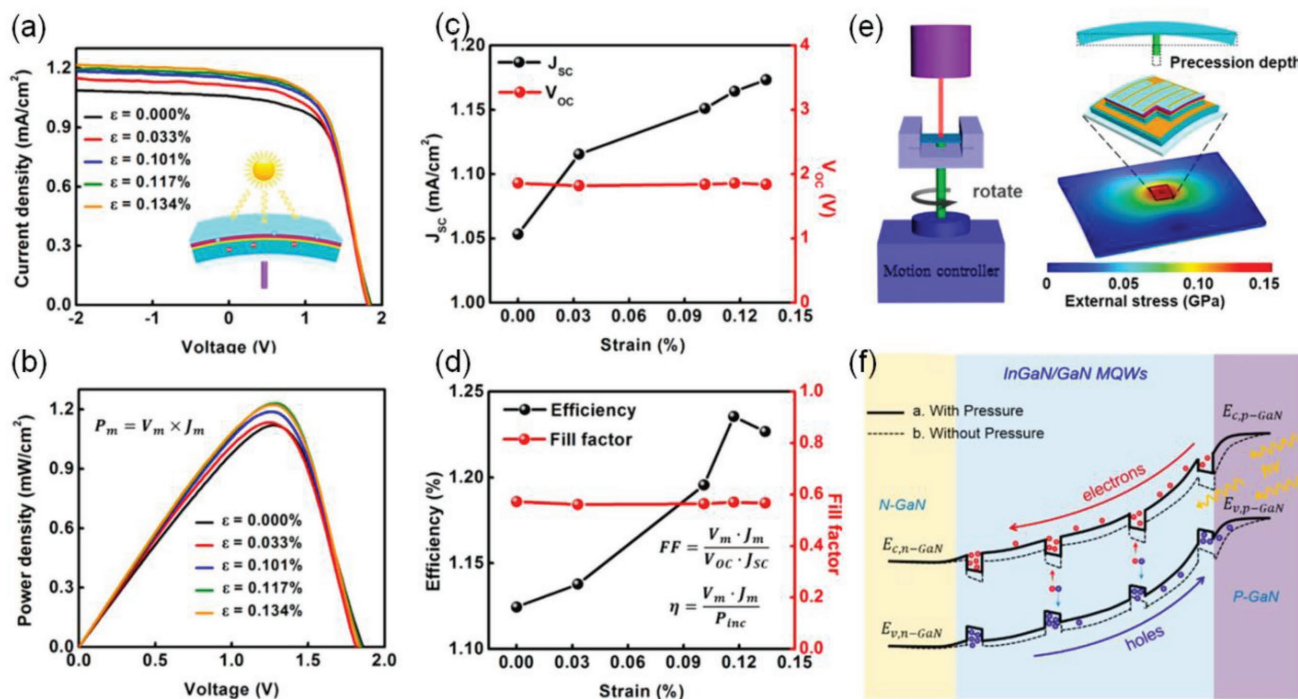


Figure 15. Piezo-phototronic effect enhanced InGaN/GaN MQW solar cell. a) J - V characteristics of the strain-modulated solar cell. b) P - V characteristics of the solar cell at different external strains. c) External strain dependence of the J_{sc} and the V_{oc} . d) Strain dependence of the efficiency and the fill factor. e) Calculated pressure distribution using COMSOL. f) Modulated energy band under a pressure. The solid line indicates the band with a pressure. Reproduced with permission.^[40] Copyright 2017, ACS.

enhances the device performances through a simple bending or pressing. The common solar cell technologies in combination with the piezo-phototronic effect will give a new insight in the progress of new generation PV technologies. Especially for commercial solar cells (such as monocrystalline silicon, CIGS, and perovskite), a little enhancement in the efficiency using piezo-phototronic effect will have a big economic influence and practical significance. High-efficiency piezoelectric solar cells can seek out applications in large-scale energy converting equipments for the national grid.

With the development of this piezoelectric effect on large-scale PV materials, the piezo-phototronic effect elevated solar cells can be put into use soon by advanced structure designs and further improved material quality. In the fundamental physical processes, only the structural, energetic, and dynamic factors of the PV devices need to be considered. However, the whole grand blueprint in the photovoltaic industry also needs to balance many practical factors, such as the cost, device lifetime, payback time, environmental impacts, and overall elemental abundance.

Acknowledgements

This research was supported by the National Key R & D Project from Minister of Science and Technology (Grant No. 2016YFA0202704), Beijing Municipal Science & Technology Commission (Grant Nos. Z171100000317001, Z171100002017017, and Y3993113DF), National Natural Science Foundation of China (Grant Nos. 11704032, 51432005, 5151101243, and 51561145021).

Conflict of Interest

The authors declare no conflict of interest.

Keywords

flexible devices, piezo-phototronic effect, piezopotential, solar cells, third generation semiconductors

Received: November 20, 2018

Revised: December 6, 2018

Published online:

- [1] A. K. Akella, R. P. Saini, M. P. Sharma, *Renewable Energy* **2009**, *34*, 390.
- [2] W. C. Turkenburg, *Renewable Energy Technologies, World Energy Assessment: Energy and the Challenge of Sustainability*, UNDP/UNDESA/WEC, New York **2000**.
- [3] W. Shockley, H. J. Queisser, *J. Appl. Phys.* **1961**, *32*, 510.
- [4] A. Polman, M. Knight, E. C. Garnett, B. Ehrler, W. C. Sinke, *Science* **2016**, *352*, aad4424.
- [5] T. Tiedje, *Appl. Phys. Lett.* **1982**, *40*, 627.
- [6] U. Rau, J. H. Werner, *Appl. Phys. Lett.* **2004**, *84*, 3735.
- [7] U. Rau, U. W. Paetzold, T. Kirchartz, *Phys. Rev. B* **2014**, *90*, 035211.
- [8] J. Nelson, *The Physics of Solar Cells*, Imperial College Press, London, UK **2003**.
- [9] M.-M. Yang, D. J. Kim, M. Alexe, *Science* **2018**, *360*, 904.
- [10] A. G. Chynoweth, *Phys. Rev.* **1956**, *102*, 705.
- [11] M. A. Green, S. P. Bremner, *Nat. Mater.* **2017**, *16*, 23.

- [12] Z. L. Wang, *Mater. Today* **2007**, *10*, 20.
- [13] Z. L. Wang, *Nano Today* **2010**, *5*, 540.
- [14] Z. L. Wang, *Adv. Mater.* **2012**, *24*, 4632.
- [15] W. Wu, Z. L. Wang, *Nat. Rev. Mater.* **2016**, *1*, 16031.
- [16] C. Du, W. Hu, Z. L. Wang, *Adv. Eng. Mater.* **2018**, *20*, 1700760.
- [17] Y. Liu, Y. Zhang, Q. Yang, S. Niu, Z. L. Wang, *Nano Energy* **2015**, *14*, 257.
- [18] Y. Dai, X. Wang, W. Peng, C. Wu, Y. Ding, K. Dong, Z. L. Wang, *Nano Energy* **2018**, *44*, 311.
- [19] Z. Wang, R. Yu, X. Wen, Y. Liu, C. Pan, W. Wu, Z. L. Wang, *ACS Nano* **2014**, *8*, 12866.
- [20] M. Chen, C. Pan, T. Zhang, X. Li, R. Liang, Z. L. Wang, *ACS Nano* **2016**, *10*, 6074.
- [21] X. Li, M. Chen, R. Yu, T. Zhang, D. Song, R. Liang, Q. Zhang, S. Cheng, L. Dong, A. Pan, Z. L. Wang, J. Zhu, C. Pan, *Adv. Mater.* **2015**, *27*, 4447.
- [22] M. Peng, Y. Liu, A. Yu, Y. Zhang, C. Liu, J. Liu, W. Wu, K. Zhang, X. Shi, J. Kou, J. Zhai, Z. L. Wang, *ACS Nano* **2016**, *10*, 1572.
- [23] L. Zhu, Y. Zhang, P. Lin, Y. Wang, L. Yang, L. Chen, L. Wang, B. Chen, Z. L. Wang, *ACS Nano* **2018**, *12*, 1811.
- [24] Z. L. Wang, *Piezo-Phototronic Effect on Solar Cells*, Springer, Berlin, Germany **2012**, p. 153.
- [25] M. Que, R. Zhou, X. Wang, Z. Yuan, G. Hu, C. Pan, *J. Phys.: Condens. Matter* **2016**, *28*, 433001.
- [26] Z. L. Wang, J. Song, *Science* **2006**, *312*, 242.
- [27] Z. Gao, J. Zhou, Y. Gu, P. Fei, Y. Hao, G. Bao, Z. L. Wang, *J. Appl. Phys.* **2009**, *105*, 113707.
- [28] Y. Gao, Z. L. Wang, *Nano Lett.* **2007**, *7*, 2499.
- [29] C. Sun, J. Shi, X. Wang, *J. Appl. Phys.* **2010**, *108*, 034309.
- [30] S. S. Lin, J. I. Hong, J. H. Song, Y. Zhu, H. P. He, Z. Xu, Y. G. Wei, Y. Ding, R. L. Snyder, Z. L. Wang, *Nano Lett.* **2009**, *9*, 3877.
- [31] W. Wu, L. Wang, Y. Li, F. Zhang, L. Lin, S. Niu, D. Chenet, X. Zhang, Y. Hao, T. F. Heinz, J. Hone, Z. L. Wang, *Nature* **2014**, *514*, 470.
- [32] L. Chen, F. Xue, X. Li, X. Huang, L. Wang, J. Kou, Z. L. Wang, *ACS Nano* **2016**, *10*, 1546.
- [33] F. Bonaccorso, L. Colombo, G. Yu, M. Stoller, V. Tozzini, A. C. Ferrari, R. S. Ruoff, V. Pellegrini, *Science* **2015**, *347*, 1246501.
- [34] D. Q. Zheng, Z. Zhao, R. Huang, J. Nie, L. Li, Y. Zhang, *Nano Energy* **2017**, *32*, 448.
- [35] X. Wen, W. Wu, Y. Ding, Z. L. Wang, *Adv. Mater.* **2013**, *25*, 3371.
- [36] X. Wen, W. Wu, Z. L. Wang, *Nano Energy* **2013**, *2*, 1093.
- [37] J. Shi, P. Zhao, X. Wang, *Adv. Mater.* **2013**, *25*, 916.
- [38] S. A. Kazazis, E. Papadomanolaki, E. Iliopoulos, *IEEE J. Photovoltaics* **2018**, *8*, 118.
- [39] S. R. Rouray, T. R. Lenka, *Micro Nano Lett.* **2017**, *12*, 924.
- [40] C. Jiang, L. Jing, X. Huang, M. Liu, C. Du, T. Liu, X. Pu, W. Hu, Z. L. Wang, *ACS Nano* **2017**, *11*, 9405.
- [41] H. Tang, B. Liu, T. Wang, *J. Phys. D: Appl. Phys.* **2015**, *48*, 025101.
- [42] R. Belghouthi, S. Taamalli, F. Echouchene, H. Mejri, H. Belmabrouk, *Mater. Sci. Semicond. Process.* **2015**, *40*, 424.
- [43] S. M. Sze, K. K. Ng, *Physics of Semiconductor Devices*, John Wiley & Sons, Hoboken, NJ, USA **2006**.
- [44] R. T. Tung, *Appl. Phys. Rev.* **2014**, *1*, 011304.
- [45] F. Léonard, J. Tersoff, *Phys. Rev. Lett.* **2000**, *84*, 4693.
- [46] F. J. Himpsel, G. Hollinger, R. A. Pollak, *Phys. Rev. B* **1983**, *28*, 7014.
- [47] R. T. Tung, *Phys. Rev. Lett.* **2000**, *84*, 6078.
- [48] J. Kang, W. Liu, D. Sarkar, D. Jena, K. Banerjee, *Phys. Rev. X* **2014**, *4*, 031005.
- [49] Y. Liu, S. Niu, Q. Yang, D. B. Klein Benjamin, Y. S. Zhou, Z. L. Wang, *Adv. Mater.* **2014**, *26*, 7209.
- [50] Z. L. Wang, W. Wu, *Natl. Sci. Rev.* **2014**, *1*, 62.
- [51] M. Amjadi, K.-U. Kyung, I. Park, M. Sitti, *Adv. Funct. Mater.* **2016**, *26*, 1678.
- [52] Y. Zhang, Z. L. Wang, *Adv. Mater.* **2012**, *24*, 4712.
- [53] Y. Zhang, Y. Yang, Z. L. Wang, *Energy Environ. Sci.* **2012**, *5*, 6850.
- [54] Y. Yang, W. Guo, Y. Zhang, Y. Ding, X. Wang, Z. L. Wang, *Nano Lett.* **2011**, *11*, 4812.
- [55] F. Boxberg, N. Søndergaard, H. Q. Xu, *Nano Lett.* **2010**, *10*, 1108.
- [56] Y. Wang, D. Zheng, L. Li, Y. Zhang, *ACS Appl. Energy Mater.* **2018**, *1*, 3063.
- [57] K. Gu, D. Zheng, L. Li, Y. Zhang, *RSC Adv.* **2018**, *8*, 8694.
- [58] R.-E. Nowak, M. Vehse, O. Sergeev, K. von Maydell, C. Agert, *Sol. Energy Mater. Sol. Cells* **2014**, *125*, 305.
- [59] L. Aé, D. Kieven, J. Chen, R. Klenk, T. Rissom, Y. Tang, M. C. Lux-Steiner, *Prog. Photovoltaics* **2010**, *18*, 209.
- [60] M. L. Brongersma, Y. Cui, S. Fan, *Nat. Mater.* **2014**, *13*, 451.
- [61] S. Qiao, J. Liu, G. Fu, K. Ren, Z. Li, S. Wang, C. Pan, *Nano Energy* **2018**, *49*, 508.
- [62] L. Zhu, L. Wang, C. Pan, L. Chen, F. Xue, B. Chen, L. Yang, L. Su, Z. L. Wang, *ACS Nano* **2017**, *11*, 1894.
- [63] G. Hu, W. Guo, R. Yu, X. Yang, R. Zhou, C. Pan, Z. L. Wang, *Nano Energy* **2016**, *23*, 27.
- [64] C. Pan, S. Niu, Y. Ding, L. Dong, R. Yu, Y. Liu, G. Zhu, Z. L. Wang, *Nano Lett.* **2012**, *12*, 3302.
- [65] A. Luque, A. Martí, *Phys. Rev. Lett.* **1997**, *78*, 5014.
- [66] L. Seunga, H. Yoshio, A. Hiroshi, *J. Phys. D: Appl. Phys.* **2016**, *49*, 025103.
- [67] E. Ertekin, P. A. Greaney, D. C. Chrzan, T. D. Sands, *J. Appl. Phys.* **2005**, *97*, 114325.
- [68] F. Glas, *Phys. Rev. B* **2006**, *74*, 121302.
- [69] F. Boxberg, N. Søndergaard, H. Q. Xu, *Adv. Mater.* **2012**, *24*, 4692.
- [70] P. J. Pauzauskie, P. Yang, *Mater. Today* **2006**, *9*, 36.
- [71] C. N. R. Rao, F. L. Deepak, G. Gundiah, A. Govindaraj, *Prog. Solid State Chem.* **2003**, *31*, 5.
- [72] Y. Dong, B. Tian, T. J. Kempa, C. M. Lieber, *Nano Lett.* **2009**, *9*, 2183.
- [73] B. Hua, J. Motohisa, Y. Kobayashi, S. Hara, T. Fukui, *Nano Lett.* **2009**, *9*, 112.
- [74] N. Sköld, L. S. Karlsson, M. W. Larsson, M.-E. Pistol, W. Seifert, J. Trägårdh, L. Samuelson, *Nano Lett.* **2005**, *5*, 1943.
- [75] P. D. C. King, T. D. Veal, P. H. Jefferson, C. F. McConville, H. Lu, W. J. Schaff, *Phys. Rev. B* **2007**, *75*, 115312.
- [76] G. Tourbot, C. Bougerol, A. Grenier, M. D. Hertog, D. Sam-Giao, D. Cooper, P. Gilet, B. Gayral, B. Daudin, *Nanotechnology* **2011**, *22*, 075601.
- [77] S. D. Carnevale, T. F. Kent, P. J. Phillips, M. J. Mills, S. Rajan, R. C. Myers, *Nano Lett.* **2012**, *12*, 915.
- [78] A. T. M. Golam Sarwar, R. C. Myers, *Appl. Phys. Lett.* **2012**, *101*, 143905.
- [79] H. Wang, H. Feng, J. Li, *Small* **2014**, *10*, 2165.
- [80] S. Wi, H. Kim, M. Chen, H. Nam, L. J. Guo, E. Meyhofer, X. Liang, *ACS Nano* **2014**, *8*, 5270.
- [81] M.-L. Tsai, S.-H. Su, J.-K. Chang, D.-S. Tsai, C.-H. Chen, C.-I. Wu, L.-J. Li, L.-J. Chen, J.-H. He, *ACS Nano* **2014**, *8*, 8317.
- [82] M. Bernardi, M. Palummo, J. C. Grossman, *Nano Lett.* **2013**, *13*, 3664.
- [83] S. Bertolazzi, J. Brivio, A. Kis, *ACS Nano* **2011**, *5*, 9703.
- [84] W. Wu, L. Wang, R. Yu, Y. Liu, S. H. Wei, J. Hone, Z. L. Wang, *Adv. Mater.* **2016**, *28*, 8463.
- [85] P. Lin, L. Zhu, D. Li, L. Xu, C. Pan, Z. Wang, *Adv. Funct. Mater.* **2018**, *28*, 1802849.
- [86] Y. Rakita, O. Bar-Elli, E. Meirzadeh, H. Kaslasi, Y. Peleg, G. Hodes, I. Lubomirsky, D. Oron, D. Ehre, D. Cahen, *Proc. Natl. Acad. Sci. USA* **2017**, *114*, E5504.
- [87] J.-H. Eom, H.-J. Choi, S. V. N. Pammi, V.-D. Tran, Y.-J. Kim, H.-J. Kim, S.-G. Yoon, *J. Phys. Chem. C* **2018**, *6*, 2786.

- [88] M. Coll, A. Gomez, E. Mas-Marza, O. Almora, G. Garcia-Belmonte, M. Campoy-Quiles, J. Bisquert, *J. Phys. Chem. Lett.* **2015**, *6*, 1408.
- [89] Y.-J. Kim, T.-V. Dang, H.-J. Choi, B.-J. Park, J.-H. Eom, H.-A. Song, D. Seol, Y. Kim, S.-H. Shin, J. Nah, S.-G. Yoon, *J. Mater. Chem. A* **2016**, *4*, 756.
- [90] S. Liu, F. Zheng, I. Grinberg, A. M. Rappe, *J. Phys. Chem. Lett.* **2016**, *7*, 1460.
- [91] I. J. Kramer, G. Moreno-Bautista, J. C. Minor, D. Kopilovic, E. H. Sargent, *Appl. Phys. Lett.* **2014**, *105*, 163902.
- [92] Y. Li, L. Wei, C. Wu, C. Liu, Y. Chen, H. Liu, J. Jiao, L. Mei, *J. Mater. Chem. A* **2014**, *2*, 15546.
- [93] G. I. Koleilat, L. Levina, H. Shukla, S. H. Myrskog, S. Hinds, A. G. Pattantyus-Abraham, E. H. Sargent, *ACS Nano* **2008**, *2*, 833.
- [94] J. Tang, E. H. Sargent, *Adv. Mater.* **2011**, *23*, 12.
- [95] Y. Cho, P. Giraud, B. Hou, Y.-W. Lee, J. Hong, S. Lee, S. Pak, J. Lee, J. E. Jang, S. M. Morris, J. I. Sohn, S. Cha, J. M. Kim, *Adv. Energy Mater.* **2018**, *8*, 1700809.
- [96] A. H. Ip, S. M. Thon, S. Hoogland, O. Voznyy, D. Zhitomirsky, R. Debnath, L. Levina, L. R. Rollny, G. H. Carey, A. Fischer, K. W. Kemp, I. J. Kramer, Z. Ning, A. J. Labelle, K. W. Chou, A. Amassian, E. H. Sargent, *Nat. Nanotechnol.* **2012**, *7*, 577.
- [97] D. A. R. Barkhouse, I. J. Kramer, X. Wang, E. H. Sargent, *Opt. Express* **2010**, *18*, A451.
- [98] B. Tian, X. Zheng, T. J. Kempa, Y. Fang, N. Yu, G. Yu, J. Huang, C. M. Lieber, *Nature* **2007**, *449*, 885.
- [99] J. Tang, Z. Huo, S. Brittman, H. Gao, P. Yang, *Nat. Nanotechnol.* **2011**, *6*, 568.
- [100] B. M. Kayes, H. A. Atwater, N. S. Lewis, *J. Appl. Phys.* **2005**, *97*, 114302.
- [101] M. Law, L. E. Greene, J. C. Johnson, R. Saykally, P. Yang, *Nat. Mater.* **2005**, *4*, 455.
- [102] Y. Tak, S. J. Hong, J. S. Lee, K. Yong, *J. Mater. Chem.* **2009**, *19*, 5945.
- [103] Y. Hu, Y. Zhang, Y. Chang, R. L. Snyder, Z. L. Wang, *ACS Nano* **2010**, *4*, 4220.
- [104] L. J. Lauhon, M. S. Gudiksen, D. Wang, C. M. Lieber, *Nature* **2002**, *420*, 57.
- [105] G. Hajime, N. Katsutoshi, T. Katsuhiko, H. Shinjiro, H. Kenji, M. Junichi, F. Takashi, *Appl. Phys. Express* **2009**, *2*, 035004.
- [106] D. H. Son, S. M. Hughes, Y. Yin, A. P. Alivisatos, *Science* **2004**, *306*, 1009.
- [107] R. D. Robinson, B. Sadtler, D. O. Demchenko, C. K. Erdonmez, L.-W. Wang, A. P. Alivisatos, *Science* **2007**, *317*, 355.
- [108] H. Li, X. Wang, J. Xu, Q. Zhang, Y. Bando, D. Golberg, Y. Ma, T. Zhai, *Adv. Mater.* **2013**, *25*, 3017.
- [109] E. D. Spoecker, M. T. Lloyd, E. M. McCready, D. C. Olson, Y.-J. Lee, J. W. P. Hsu, *Appl. Phys. Lett.* **2009**, *95*, 213506.
- [110] B. Sun, Y. Hao, F. Guo, Y. Cao, Y. Zhang, Y. Li, D. Xu, *J. Phys. Chem. C* **2012**, *116*, 1395.
- [111] Q. Cui, C. Liu, F. Wu, W. Yue, Z. Qiu, H. Zhang, F. Gao, W. Shen, M. Wang, *J. Phys. Chem. C* **2013**, *117*, 5626.
- [112] Y. Gao, Z. L. Wang, *Nano Lett.* **2009**, *9*, 1103.
- [113] C. Zuo, J. Bolink Henk, H. Han, J. Huang, D. Cahen, L. Ding, *Adv. Sci.* **2016**, *3*, 1500324.
- [114] S. D. Stranks, G. E. Eperon, G. Grancini, C. Menelaou, M. J. P. Alcocer, T. Leijtens, L. M. Herz, A. Petrozza, H. J. Snaith, *Science* **2013**, *342*, 341.
- [115] J.-Y. Jeng, Y.-F. Chiang, M.-H. Lee, S.-R. Peng, T.-F. Guo, P. Chen, T.-C. Wen, *Adv. Mater.* **2013**, *25*, 3727.
- [116] M. M. Lee, J. Teuscher, T. Miyasaka, T. N. Murakami, H. J. Snaith, *Science* **2012**, *338*, 643.
- [117] C. C. Stoumpos, C. D. Malliakas, M. G. Kanatzidis, *Inorg. Chem.* **2013**, *52*, 9019.
- [118] M. V. Kovalenko, L. Protesescu, M. I. Bodnarchuk, *Science* **2017**, *358*, 745.
- [119] Z. Wang, R. Yu, C. Pan, Z. Li, J. Yang, F. Yi, Z. L. Wang, *Nat. Commun.* **2015**, *6*, 8401.
- [120] J. Berry, T. Buonassisi, D. A. Egger, G. Hodes, L. Kronik, Y.-L. Loo, I. Lubomirsky, S. R. Marder, Y. Mastai, J. S. Miller, D. B. Mitzi, Y. Paz, A. M. Rappe, I. Riess, B. Rybtchinski, O. Stafsudd, V. Stevanovic, M. F. Toney, D. Zitoun, A. Kahn, D. Ginley, D. Cahen, *Adv. Mater.* **2015**, *27*, 5102.
- [121] C. Battaglia, C.-M. Hsu, K. Söderström, J. Escarré, F.-J. Haug, M. Charrière, M. Boccard, M. Despeisse, D. T. L. Alexander, M. Cantoni, Y. Cui, C. Ballif, *ACS Nano* **2012**, *6*, 2790.
- [122] P. H. Wang, R.-E. Nowak, S. Geißendörfer, M. Vehse, N. Reininghaus, O. Sergeev, K. von Maydell, A. G. Brolo, C. Agert, *Appl. Phys. Lett.* **2014**, *105*, 183106.
- [123] Y.-J. Lee, D. S. Ruby, D. W. Peters, B. B. McKenzie, J. W. P. Hsu, *Nano Lett.* **2008**, *8*, 1501.
- [124] M. A. Green, *Prog. Photovoltaics* **2009**, *17*, 183.
- [125] J. Bullock, M. Hettick, J. Geissbühler, A. J. Ong, T. Allen, C. M. Sutterfella, T. Chen, H. Ota, E. W. Schaler, S. D. Wolf, C. Ballif, A. Cuevas, A. Javey, *Nat. Energy* **2016**, *1*, 15031.
- [126] Z. Shao, L. Wen, D. Wu, X. Zhang, S. Chang, S. Qin, *J. Appl. Phys.* **2010**, *108*, 124312.
- [127] A. Chirilă, S. Buecheler, F. Pianezzi, P. Bloesch, C. Gretener, A. R. Uhl, C. Fella, L. Kranz, J. Perrenoud, S. Seyrling, R. Verma, S. Nishiwaki, Y. E. Romanyuk, G. Bilger, A. N. Tiwari, *Nat. Mater.* **2011**, *10*, 857.
- [128] K. L. Chopra, P. D. Paulson, V. Dutta, *Prog. Photovoltaics* **2004**, *12*, 69.
- [129] L. Zhu, P. Lin, B. Chen, L. Wang, L. Chen, D. Li, Z. L. Wang, *Nano Res.* **2018**, *11*, 3877.
- [130] L. Cao, J.-S. Park, P. Fan, B. Clemens, M. L. Brongersma, *Nano Lett.* **2010**, *10*, 1229.
- [131] A. B. Wong, S. Brittman, Y. Yu, N. P. Dasgupta, P. Yang, *Nano Lett.* **2015**, *15*, 4096.
- [132] L. Zhu, L. Wang, F. Xue, L. Chen, J. Fu, X. Feng, T. Li, Z. L. Wang, *Adv. Sci.* **2017**, *4*, 1600185.
- [133] S. Shoaee, J. Briscoe, J. R. Durrant, S. Dunn, *Adv. Mater.* **2014**, *26*, 263.
- [134] M. S. Lohse, T. Bein, *Adv. Funct. Mater.* **2018**, *28*, 1705553.